frontiers | Frontiers in Earth Science

ORIGINAL RESEARCH
published: 04 July 2022
doi: 10.3389/feart.2022.881080

Early Cretaceous Slump Deposits in Laiyang Group (Lingshan Island, East China): New Constraints for Provenance Identification and Tectonic Evolution

*Yuzhe Wang, Longwei Qiu *, Yongqiang Yang, Baoliang Yang, Daotao Dong, Danish Khan and Zhongren Guo*

School of Geosciences, China University of Petroleum (East China), Qingdao, China

The sedimentary strata in the Lingshan Island area are gaining attention because of their unique sedimentary and tectonic characteristics. However, the provenance and the depositional and tectonic setting in this area remain the focus of controversy. There is a significant slump deposit with lateral length up to 250 m in the Laohuzui section at the top of the Laiyang Group, which differs from the underlying turbidite deposits in morphology and composition. The sandstone in the Laohuzui section was continuously sampled and analyzed for major trace and rare earth elements. The results showed that the Laohuzui section is mixed with a continental margin provenance from the re-cyclic deposition in the arid region, which is different from the continental island arc provenance in the lower part of the Laiyang Group. Through the geochemical study of the igneous gravel contained in the olistolite and the comparison with the igneous rocks in the surrounding area, it is observed that the properties of the igneous gravel are most like those of the igneous rock deposit in the Zhucheng-Taolin area. In addition, the Lingshan Island and the Zhucheng-Taolin areas have similar sedimentary processes, suggesting that both received provenance from the Jiaonan uplift at the end of the Early Cretaceous. This study clarified the depositional processes of the later period of the Laiyang Group deposition in the Lingshan Island area.

Keywords: Laiyang Group, slump deposit, geochemistry, provenance, tectonic evolution

OPEN ACCESS

Edited by:
Guillermo Booth-Rea, University of Granada, Spain

Reviewed by:
Avraam Zelilidis, University of Patras, Greece
Mohammad Adnan Quasim, Aligarh Muslim University, India

****Correspondence:***
Longwei Qiu
qiulwsd@163.com

Specialty section:
This article was submitted to Structural Geology and Tectonics, a section of the journal Frontiers in Earth Science

Received: *23 February 2022*
Accepted: *19 May 2022*
Published: *04 July 2022*

Citation:
Wang Y, Qiu L, Yang Y, Yang B, Dong D, Khan D and Guo Z (2022) Early Cretaceous Slump Deposits in Laiyang Group (Lingshan Island, East China): New Constraints for Provenance Identification and Tectonic Evolution. Front. Earth Sci. 10:881080. doi: 10.3389/feart.2022.881080

1 INTRODUCTION

The sedimentary sequence of a basin can inherit the tectonic background, sedimentary environment, and even the characteristics of paleoclimate conditions during the formation of the parent rocks. Consequently, provenance analysis is a crucial method for unraveling the sediment deposition and the tectonic activity (Bahlburg et al., 2010; Fan et al., 2019; Yang et al., 2019). Geochemical analyses have long been utilized to investigate the provenance of siliciclastic rocks (Armstrong-Altrin et al., 2004; Moosavirad et al., 2011; Zhang et al., 2018). The tectonic setting can be deduced by the geochemical characteristics of the siliciclastic sediments (Bhatia, 1983; Bhatia and Crook, 1986; Mclennan and Taylor, 1991; Khan et al., 2020; Ahmad et al., 2022). A combination of several elemental geochemical proxies such as Chemical Index of Alteration (CIA) (Nesbitt and Young, 1982) and index component variation (ICV) (Cox et al., 1995) is widely adopted to infer the weathering intensity of the source area

(Xiaoping et al., 2012). Specific ratios of trace elements, for instance, Sr/Ba, Sr/Cu, Th/U, and Ni/Co, can reflect the paleoclimate, paleosalinity, and redox conditions faithfully.

The Lingshan Island is situated in the Sulu orogenic belt, formed by the collision between the North China Craton and the Yangtze Craton during the Late Triassic (**Figure 1A**). The sediments of the Lingshan Island are developed in the transitional period between the siltstone from the late Laiyang Group and the igneous rock from the early Qingshan Group. Although the regional stress fields of the Laiyang Group and Qingshan Group are generally in the tensile stress field, a rapid tectonic inversion occurred at about 125 Ma and received a brief compressive stress field (**Figure 2**) (Zhou et al., 2015). Such characteristics enable the sediments in the Lingshan Island area to reflect the tectonic activity and sedimentary environment of the Sulu orogenic belt in the Early Cretaceous. Previous studies regarded the Laiyang Group of the Lingshan Island area as the outer fan of submarine fans developed in a marine environment due to the development of flysch, synsedimentary collapse fold structures, synsedimentary deformation structures, analysis of microfossils, and the interbedding between thin sand, silt, and black shale (Lu et al., 2011, 2012, 2013). The geochemical data also show that the siltstone of the Laiyang Group was deposited in an arid, reducing marine environment (Zhang et al., 2017). However, the imbricate-like structures, groove patterns, and carbon debris development in the Laiyang Group of Lingshan Island are well developed (Zhong, 2012; Zhong et al., 2016), combined with the discovery of the typical lacustrine fauna fish fossils of the Jehol biota (Li et al., 2017) and the continuity of stratigraphic age of the Laiyang Group and Qingshan Group (Meng et al., 2018), and all indicate that the study area may be continental lacustrine shallow-water delta deposits. Although researchers have carried out more research studies on Lingshan Island, there is still controversy in provenance, sedimentary environment, and tectonic setting. In addition, previous studies have mainly focused on the Laiyang Group and Qingshan Group itself, while the slump deposits developed in the transitional zone between them have not received much attention so far.

The provenance, sedimentary environment, and tectonic environment of Lingshan Island are pivotal in resolving the controversies. Therefore, the author selected development in the transitional stage of the Laohuzui section as the research object, using unmanned aerial vehicle (UAV) laser radar 3D modeling and geochemical test. Restoring the sedimentary process occurring between the transition stage of the late Laiyang Group and Qingshan Group provides new evidence for the study of sedimentary, tectonic environment, and provenance analysis.

2 GEOLOGICAL BACKGROUND

Lingshan Island is the largest island in northern China, located 22 nautical miles south of Qingdao in Shandong

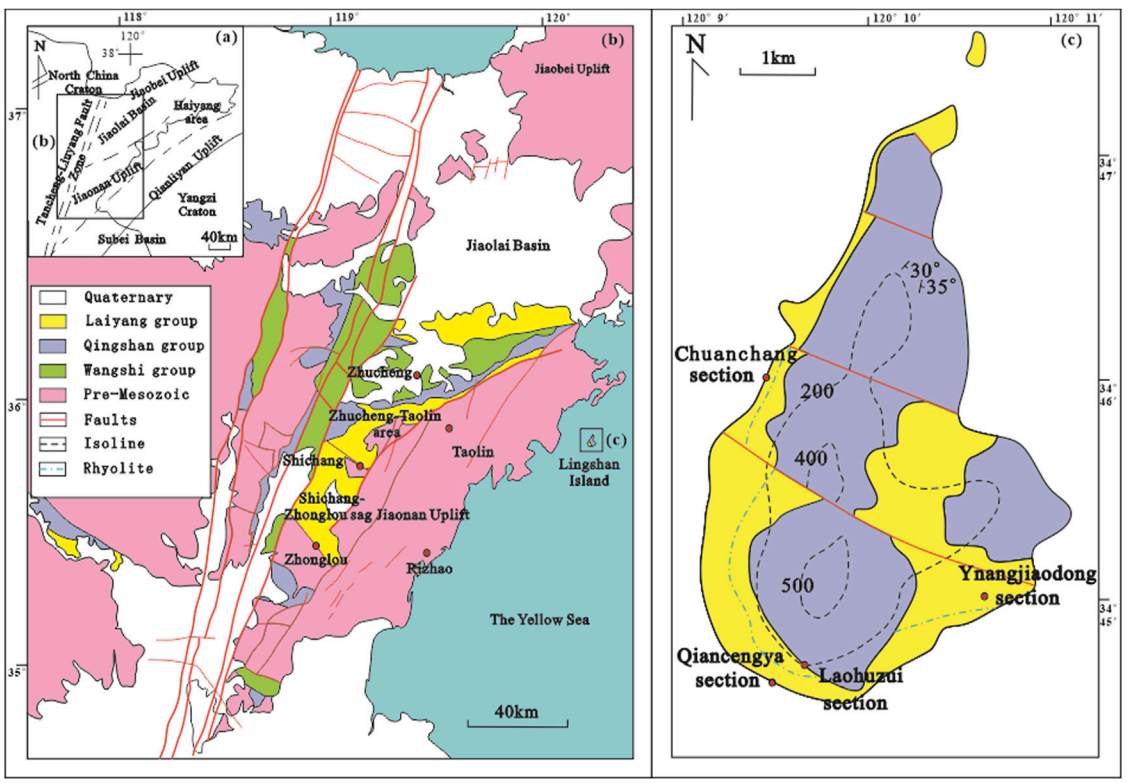

FIGURE 1 | Geotectonic location and geological schematic diagram of Lingshan Island. **(A,B)** Location and tectonic setting around Lingshan Island, modified after Shen et al. (2016) and Zhang et al. (2017). **(C)** The geological sketch map of Lingshan Island, modified after Luan et al. (2010).

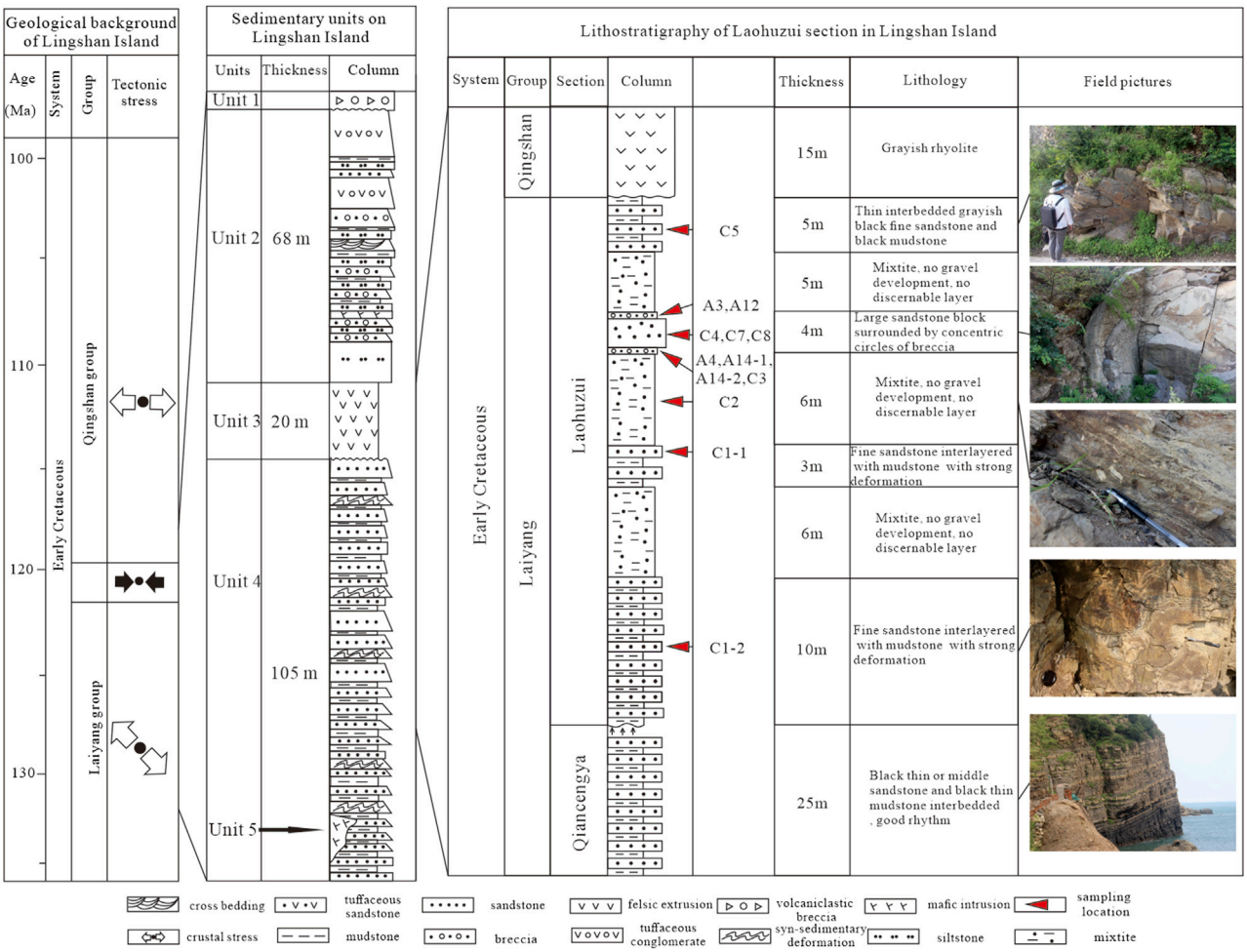

FIGURE 2 | Comprehensive strata log diagram of the Laohuzui section in Lingshan Island, the geological background modified after Zhou et al. (2015), and the sedimentary units of Lingshan Island modified after Wang J et al. (2014). The deformation degree of the strata gradually enhanced upward and transformed into mixed accumulation near the unconformity surface between the Laiyang Group and Qingshan Group.

province (**Figure 1**). Lingshan Island is composed of the Laiyang Group and Qingshan Group, separated by an unconformity marked by a set of thick pale off-white cryptocrystalline rhyolites. The strata of the Laiyang Group developed in the lower part of the island, and the layer above the sea is about 105 m thick, composed of thin gray sandstone and black mudstone (**Figure 2**) (Wang J et al., 2014). Fossils are rare in this area, and sporopollenin, sporadic dinoflagellates, and membranous algae fragments were only found in a few samples (Lu et al., 2011; Dong, 2014; Zhou et al., 2015). The upper Qingshan Group sediments are about 80 m thick, with complex lithology and variable occurrence, and are composed of volcanic rock and pyroclastic rock (**Figure 2**) (Wang J et al., 2014).

There are several sections of the Laiyang Group strata on Lingshan Island. Most sections, such as the Qiancengya section, consist of dark gray siltstone alteration with thin black mudstone; the collapse fold and soft sedimentary deformation are developed, but they are all confined within the layer (**Figure 2**).

The Laohuzui section, located in the southernmost part of Lingshan Island, extends horizontally for about 250 m. As the section closest to the unconformity surface, all the layers are strongly modified and different degrees of deformation occurs between layers (**Figure 2**). The sedimentary characteristics and composition of the section are quite different from the other section in the lower part of the Laiyang Group.

3 MATERIALS AND METHODS

In order to reflect the geochemical changes of the Laohuzui section and analyze the possible pattern, unmanned aerial vehicle radar technology was used to conduct 3D modeling of the Laohuzui section (**Figures 3B–E**), and the characteristics of the profile were analyzed. On this basis, the samples were collected from the Laohuzui section.

In order to fully reflect the nature of the provenance area, nine fresh siltstone samples with similar particle sizes were taken from

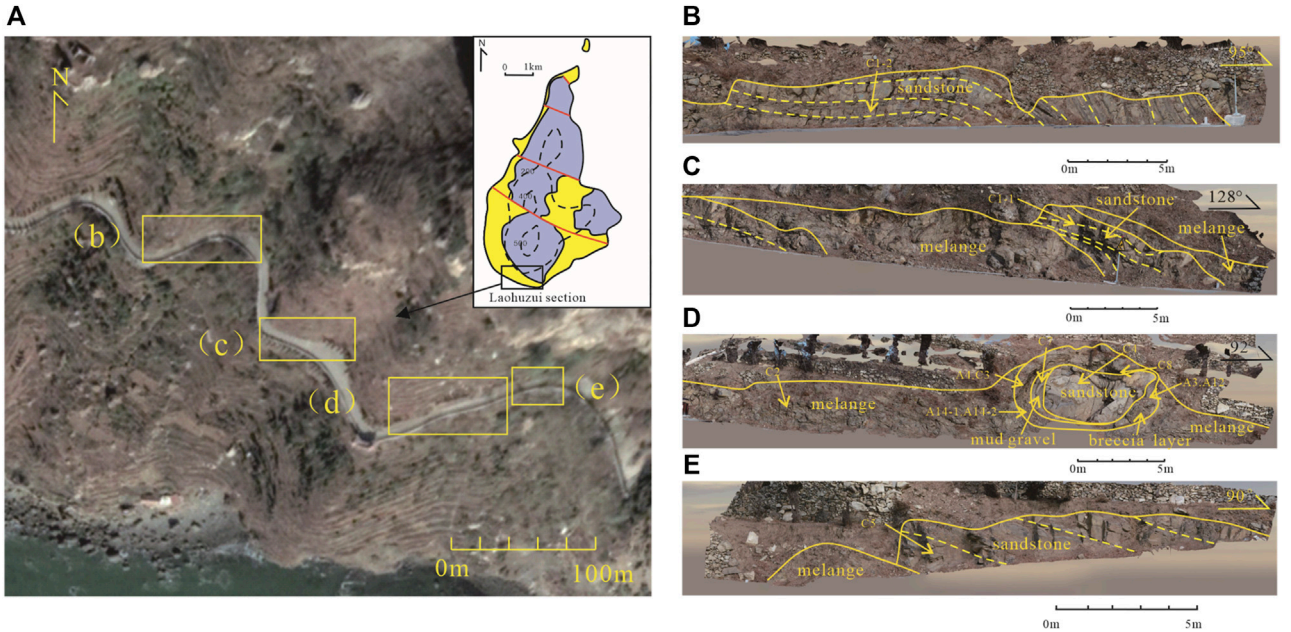

FIGURE 3 | Distribution of the Laohuzui section and sampling sites. **(A)** The location of a laser radar 3D model and photo image from Google Earth, **(B)** stratum is still relatively flat at the western-most side of the Laohuzui section, **(C)** the melange have been well developed in the middle of the Laohuzui section , **(D)** the eastern part of the Laohuzui section is entirely composed of melange, a large olistolite with sandstone block developed within, and **(E)** the stratum is restored to flat interbedded sand and mudstone at the eastern-most side of the Laohuzui section.

the Laohuzui section, named C1-1, C1-2, C2, C3, C4, C5, C6, C7, and C8. C1-1 and C1-2 were from the sandstone in the lower part of the Laohuzui section with good stratification (**Figures 3B,C**), C2 was taken from the siltstone mixed accumulation in the lower section with suffered severe deformation and no apparent stratification, C3 was obtained from the breccia groundmass around the sandstone block, C4 was taken from the vast sandstone block itself, C7 was taken from the groundmass of the boulder clay layer around the sandstone block, and C8 was derived from the mud gravel of the boulder clay layer. A14-2 was a sandstone sample which encased the igneous gravel. The sampling sites covered all the different sediment forms in the Laohuzui section (**Figure 3D**); C5 was taken from the sandstone layer with good stratification between the Laohuzui section and the rhyolites (**Figure 3E**). Four volcanic samples (A4, A3, A14-1, and A12) were also selected from breccia in the Laohuzui section. The sampling location is shown in **Figure 3D**.

The processing and geochemical testing for samples were conducted in the Shandong Eighth Geological and Mineral Exploration Institute laboratory. The principal elements were selected by an X-ray fluorescence (XRF) spectrometer and processed according to the national standard GBT14506.28-2010 (equipment model: Axios). During this analytical process, the test material was fused with anhydrous lithium tetraborate, ammonium nitrate as the oxidizer, lithium fluoride, and a small amount of lithium bromide as flux and release agent. The mass ratio of test material to flux was 1:8. The material was melted at 1,150°C~1,250°C on the automatic fusion machine to make a thin glass section and measured on an X-ray fluorescence spectrometer. For Ni, Cu, Si, and Zr, the Compton scattering line was used as an internal standard to correct the matrix effect. For other elements, the absorption enhancement effect among the elements was corrected by theoretical theory, and the primary and secondary components were calculated according to the fluorescence intensity.

The REE and trace elements were dissolved in a closed vessel with hydrofluoric acid and nitric acid, and then the hydrofluoric acid was evaporated on the electric heating plate. After that, the leftover was sealed and dissolved with nitric acid and then directly measured by the standard external method of inductively coupled plasma mass spectrometry (ICP-MS) (equipment type: ICAP Qc) after dilution. Using the same reference material of the principal element as the quality control sample, the uncertainty for all the major/secondary elements and most trace elements was less than 5% of the measured value. The sample analysis results are shown in **Table 1**.

4 RESULTS

4.1 Sedimentary Character

The Laohuzui section is exposed east–west along the highway, divided into three sections (**Figure 3A**). Among them, the left-most stratum is seriously modified and has no fixed tendency, but the structure of interbedded sand–mudstone is still relatively complete (**Figure 3B**). The stratum deformation gradually increased and turned into mixtite to the east, and the bedding architecture could not be distinguished (**Figure 3C**). There was a

TABLE 1 | Main elements (%), trace elements, REE (PPM), and characteristic values of samples in the Laohuzui section.

Point	Siltstone										Igneous rock		
	C1-1	C1-2	C2	C3	C5	C7	C4	C8	A14-2	A4	A3	A14-1	A12
Al_2O_3	14.77	15.09	15.11	12.70	15.20	13.96	14.49	15.25	12.79	20.01	19.31	17.08	15.98
CaO	2.34	0.73	4.26	4.11	0.61	1.04	5.51	1.43	4.02	4.70	4.11	6.50	8.95
Fe_2O_3	2.50	3.54	2.47	1.44	3.24	1.80	0.92	2.75	1.55	3.02	2.43	1.40	1.85
$Fe_2O_3^T$	4.91	4.92	5.58	3.85	5.31	3.52	4.71	5.85	5.34	6.74	5.53	6.98	8.06
K_2O	3.68	3.39	3.17	2.92	3.63	3.26	2.57	3.48	2.52	2.10	1.70	2.96	3.26
MgO	2.01	1.90	3.03	2.15	2.49	1.62	3.05	3.51	2.71	2.92	1.92	3.58	4.11
MnO	0.07	0.10	0.06	0.05	0.07	0.08	0.08	0.06	0.07	0.10	0.10	0.09	0.17
Na_2O	3.04	3.18	3.00	2.71	2.66	3.40	3.91	2.70	2.75	4.92	5.43	4.82	3.48
P_2O_5	0.30	0.26	0.31	0.25	0.26	0.26	0.28	0.24	0.25	0.41	0.59	0.58	0.75
SO_3	0.06	0.01	0.00	0.04	0.01	0.02	0.20	0.01	0.05	0.08	0.26	0.84	0.75
TiO_2	0.50	0.61	0.67	0.48	0.68	0.42	0.68	0.71	0.55	1.90	0.86	0.98	1.03
LOI	4.61	3.24	6.67	6.27	3.58	2.72	7.04	5.64	6.44	4.74	2.57	6.92	9.20
SiO_2	62.91	65.78	57.34	63.67	64.69	68.89	56.67	60.32	61.73	50.57	56.82	47.87	43.47
FeO	2.17	1.24	2.79	2.17	1.86	1.55	3.41	2.79	3.41	3.72	3.10	5.58	6.21
La	46.39	46.58	52.76	41.98	57.79	46.68	54.00	54.72	52.89	67.53	46.61	63.68	72.46
Ce	96.85	91.63	101.10	77.70	104.13	86.66	97.17	97.70	93.23	128.77	104.66	125.55	148.47
Pr	12.86	11.98	13.38	10.16	13.94	11.85	12.72	13.16	11.75	17.68	13.94	17.24	21.55
Nd	46.56	43.72	47.63	35.95	49.13	40.90	44.34	46.10	39.56	64.31	53.69	62.75	86.27
Eu	2.10	1.80	1.94	1.60	1.93	1.94	1.95	1.72	1.68	6.08	2.44	3.22	4.93
Sm	8.40	8.11	8.65	6.59	8.75	7.68	7.92	8.13	6.49	12.97	10.06	11.22	18.13
Tb	0.98	1.06	1.03	0.89	1.14	0.95	0.91	1.01	0.69	2.05	1.13	1.28	2.18
Gd	6.61	6.85	6.80	5.51	7.23	6.09	6.06	6.61	4.78	12.18	7.81	8.92	15.40
Dy	4.99	5.56	5.35	4.60	5.82	5.06	4.62	5.33	3.59	11.02	5.61	6.27	10.43
Ho	0.89	1.05	0.99	0.98	1.12	0.95	0.84	1.01	0.69	2.10	0.97	1.11	1.81
Er	2.33	3.01	2.58	2.76	3.04	2.66	2.23	2.80	1.86	5.58	2.54	2.88	4.44
Tm	0.35	0.47	0.41	0.42	0.47	0.43	0.38	0.46	0.31	0.87	0.37	0.40	0.67
Yb	2.16	2.89	2.63	2.43	3.06	2.56	2.24	2.78	2.01	5.32	2.19	2.45	3.69
Lu	0.33	0.45	0.38	0.39	0.46	0.41	0.34	0.43	0.32	0.81	0.32	0.39	0.58
Y	23.65	26.84	22.02	108.83	26.24	22.44	19.15	22.81	15.62	46.73	22.81	26.32	45.58
Sc	9.14	10.75	10.93	9.54	10.54	8.18	9.40	10.77	9.70	21.60	18.22	10.56	9.67
Li	25.48	28.96	31.19	27.24	32.24	23.57	26.85	35.04	28.94	43.15	20.86	32.53	41.62
Be	1.83	2.14	2.44	2.19	2.45	1.63	1.87	3.11	1.56	2.71	1.58	0.66	1.04
Co	25.27	37.11	27.37	31.30	45.74	27.44	23.90	22.14	28.74	38.47	41.29	53.56	31.64
Ni	22.02	31.05	24.96	24.02	29.52	21.00	24.53	36.26	32.27	23.37	53.48	59.02	38.18
Cu	23.71	28.01	31.42	25.60	27.81	17.30	16.91	36.26	24.05	25.07	29.86	27.07	34.91
Zn	98.46	99.16	79.68	65.74	74.16	73.90	59.31	76.89	87.42	111.67	82.75	83.30	130.10
Ga	19.53	20.65	22.63	17.22	21.18	15.78	17.72	22.04	18.13	25.59	20.58	19.01	17.90
Rb	89.92	100.50	92.18	93.57	124.22	76.60	62.10	113.30	66.44	50.56	24.34	51.17	54.14
Sr	364.93	191.36	509.66	340.90	240.78	278.34	494.21	168.35	476.75	459.39	974.18	845.06	624.95
Cs	4.84	4.93	5.57	6.24	9.23	3.76	3.17	8.63	4.15	1.98	0.95	1.31	1.17
Ba	58.90	97.43	122.05	187.99	162.92	105.00	169.56	174.79	167.30	66.42	50.60	75.17	86.31
Pb	26.72	20.53	27.45	23.66	31.65	35.92	21.67	380.34	29.72	32.36	19.29	37.79	32.44
Th	10.35	9.35	9.80	8.62	10.48	7.51	7.81	10.13	8.12	4.45	2.37	6.59	6.46
U	1.58	1.83	1.87	2.44	2.39	2.23	1.47	1.99	1.67	1.10	0.23	1.28	2.18
Nb	11.71	14.73	13.40	9.89	14.72	9.42	12.80	13.13	11.33	40.93	10.52	14.01	13.71
Ta	4.04	4.81	4.14	3.87	4.62	2.56	4.16	4.41	3.81	13.51	2.94	3.60	3.52
Sb	0.69	0.38	0.39	0.31	0.55	0.66	0.29	0.36	0.38	0.78	0.79	1.04	0.95
Tl	0.99	0.69	0.63	0.57	0.75	0.56	0.40	0.68	0.52	0.36	0.17	0.58	0.54
Bi	0.26	0.24	0.25	0.30	0.30	0.19	0.17	0.28	0.21	0.09	0.11	0.11	0.11
B	102.00	97.60	96.80	113.00	90.20	85.50	39.90	81.20	58.50	35.90	12.10	28.80	19.20
V	83.61	91.24	116.37	98.87	92.77	69.05	105.21	119.89	119.77	253.17	182.59	114.96	99.93
Cr	43.79	62.31	54.72	66.75	61.10	49.53	68.05	81.20	62.86	74.53	148.50	85.36	64.72
As	4.00	2.60	3.70	4.30	8.20	16.10	6.30	3.40	12.50	28.30	9.60	32.70	17.00
Zr	217.00	238.70	252.70	203.30	234.00	209.00	261.60	211.40	230.00	209.00	146.70	324.40	248.90
Hf	6.79	7.44	7.07	6.61	7.26	6.61	7.07	6.23	6.79	7.63	6.79	8.47	5.77
ICV	0.96	0.89	1.10	1.09	0.88	0.83	1.15	0.96	1.11	0.98	0.86	1.19	1.43
CIA	64.68	70.10	62.25	60.39	71.62	67.07	58.22	69.15	61.43	74.02	73.04	68.71	70.33
F_1	−1.82	−2.21	−1.15	−2.21	−3.49	−2.74	−0.26	−3.90	−1.51	3.24	5.64	2.30	2.05
F_2	1.63	0.90	0.45	0.77	−0.30	1.70	1.65	−1.37	−0.73	2.68	3.54	3.11	1.71
ΣREE	231.81	225.17	245.65	191.94	258.02	214.81	235.71	241.95	219.85	337.26	252.33	307.37	391.01
LREE	213.17	203.82	225.47	173.97	235.67	195.70	218.10	221.53	205.60	297.33	231.39	283.66	351.81
HREE	18.64	21.35	20.17	17.97	22.35	19.11	17.62	20.43	14.25	39.92	20.94	23.71	39.21

(Continued on following page)

TABLE 1 | (*Continued*) Main elements (%), trace elements, REE (PPM), and characteristic values of samples in the Laohuzui section.

Point	Siltstone										Igneous rock		
	C1-1	C1-2	C2	C3	C5	C7	C4	C8	A14-2	A4	A3	A14-1	A12
LREE/HREE	11.43	9.55	11.18	9.68	10.55	10.24	12.38	10.85	14.42	7.45	11.05	11.96	8.97
δEu	1.33	1.14	1.19	1.25	1.14	1.34	1.32	1.11	1.42	2.27	1.29	1.51	1.39
δCe	0.93	0.91	0.90	0.89	0.87	0.89	0.89	0.87	0.91	1.95	2.09	1.99	1.87
Mg*	0.48	0.61	0.52	0.50	0.57	0.51	0.47	0.56	0.44	0.44	0.38	0.39	0.40
$(La/Sm)_N$	0.80	0.83	0.89	0.93	0.96	0.88	0.99	0.98	1.18	0.76	0.67	0.82	0.58
$(Gd/Yb)_N$	1.85	1.43	1.56	1.37	1.43	1.44	1.64	1.44	1.44	1.39	2.15	2.20	2.53
$(La/Yb)_N$	1.58	1.19	1.48	1.28	1.40	1.35	1.78	1.45	1.94	0.94	1.57	1.92	1.45
Ce_{anom}	−0.02	−0.04	−0.04	−0.05	−0.06	−0.05	−0.06	−0.06	−0.05	−0.05	−0.01	−0.04	−0.06

Note: (a) $Fe_2O_3^T = Fe_2O_3+1.1113\times FeO$.

(b) $F_1= (-1.773TiO_2)+ (0.607Al_2O_3)+ (0.760Fe_2O_3T)+(-1.500MgO)+(0.616CaO)+(0.509Na_2O)+(-1.224K2O)+(-9.090)$;

$F_2=(0.445TiO_2)+(0.070Al_2O_3)+(-0.250Fe_2O_3T)+(-1.142MgO)+(0.438CaO)+(1.475Na_2O)+(1.426K_2O)+(-6.861)$ *(after Roser and Korsch, 1988).*

(c) $ICV= (Fe_2O_3+K_2O + Na_2O + CaO + MgO + MnO + TiO_2)/Al_2O_3$*(percentage).*

(d) $CIA = [(Al_2O_3/(Al_2O_3+CaO^*+Na_2O + K_2O)]\times100$*(molar weight).*

(e) CaO correction according to the formula proposed by McLennan et al. (1993).*

(f) $\delta Eu = 2\times EuN/(SmN + GdN)$.

(g) $\delta Ce = 2\times Ce_N/(La_N + Nd_N)$*, where N represents standardization of PAAS, and chondrite values refer to Taylor and McLennan (1985).*

(h) $Ce_{anom} = lg[3Ce_N/(2La_N + Nd_N)]$*, where N is the standardization of North American shale, and the value of North American shale refers to Gromet et al (1985).*

(i) $Mg^* = MgO/(MgO + FeO)$.

large olistolite with a sandstone block developed in the center of the Laohuzui slump deposit, surrounded by concentric circles of breccia (**Figure 3D**). To the topmost of the section, the strata changed into flat sand and interbedded mudstone deposits (**Figure 3E**). The overlying strata are the unconformities and rhyolite deposited as the boundary between Laiyang and Qingshan Groups.

Based on field observations, the rock slices collected from different regions were observed under the microscope (**Figure 4**), and the sampling locations are shown in **Figures 2** and **3**.

Detrital particles of sand–mudstone samples in the Laohuzui section were mainly quartz, followed by feldspar and mica, and the cementation was mainly clay minerals. Among them, C2 and C5 slices showed apparent directional arrangement (**Figure 4B**), but the remaining samples did not, indicating that the dynamic environment at different positions of the Laohuzui section is varied. The grain size also varied considerably from silty sand to medium sand, but all of them were larger than the rest of the sections of the Laiyang Group, Lingshan Island (Zhang et al., 2017). With the approach of the sandstone block, the grain size of samples increased gradually.

Debris in thin sections was mainly metamorphic rock, basalt, and occasionally planted debris. The debris content and composition were significantly different between the slices. The samples C1-1 and C1-2 were mainly quartz particles, and metamorphic debris less than 0.5 mm is occasionally seen (**Figure 4A**). Debris in the millimeter level was observed in C2 (**Figure 4B**); the samples C7 and C4 with granular metamorphic rock and igneous rock debris accounted for more than one-third (**Figures 4C,D**), which also showed that the closer to the sandstone block, the more debris there is. However, sample C5 developed in the strata above the Laohuzui section showed no debris (**Figure 4E**). The samples of igneous gravel in the study area were mainly basalt, and the elongated plagioclase microcrystals were randomly distributed inside (**Figure 4F**).

Through comprehensive analysis of the microscopic characteristics and sampling locations, it was found that there were significant differences in the mineral content, particle size, and structure for the samples of the Laohuzui section. The closer to the olistolite, the larger the particle size, and the higher the debris content. The results also show that the sediment characteristics and composition of the Laohuzui section are very different from turbidite deposits in other sections of the Laiyang Group, Lingshan Island (Zhang et al., 2017).

4.2 Geochemical Characteristics of Siltstone Samples

Siltstone data from the Laohuzui section were compared with upper continental crust (UCC) (Rudnick and Gao, 2003) and post-Archean Australian shale (PAAS) (Taylor and McLennan, 1985), demonstrating that compared with the lower strata of the Laiyang Group, Lingshan Island (Zhang et al., 2017), the contents of elements in the Laohuzui section samples are generally closer to UCC. In the Laohuzui section, SiO_2, Na_2O, K_2O, and P_2O_5 were significantly increased; however, the contents of MgO and CaO were significantly decreased, while the contents of Al_2O_3, Fe_2O_3, MnO, and TiO_2 did not significantly change. The comparison between the Laohuzui section and the lower strata of the Laiyang Group showed that the element content variation and maturity are quite different. K_2O/Na_2O can represent the relative contents of potassium feldspar and plagioclase, in which the Na_2O content in C4, C7, and A14-2 were greater than the K_2O content, and in other samples, K_2O was higher than Na_2O. The SiO_2/Al_2O_3 was 5.01–3.62, with an average of 4.31, usually indicating immature sedimentary rocks (Potter, 1978), but the maturity was significantly higher than the lower strata of the Laiyang Group in Lingshan Island (with an average of 3.78) (Zhang et al., 2017).

The standardization of trace UCC elements in siltstone samples is shown in **Figure 5A**. Large ionic lithophile

elements (LILE) are geochemically active elements, mainly represented by Cs, Rb, Sr, U, and Rb, which have shown depletion in samples C7, C4, and A14–2, while other elements exhibited weak enrichment. All samples showed weak U depletion. Sr and Cs showed different characteristics in each sample. Representative high field strength elements (HFSE) such as Nb, Ta, Zr, Hf, Th, Yb, and Y are characterized by stable geochemical properties; are not susceptible to metamorphism, alteration, and weathering; and are more abundant in felsic rocks than mafic rock(Zhang et al., 2017). In **Figure 5A**, Nb, Yb, Hf, Y, and Zr elements generally showed weak enrichment; Ta showed strong enrichment; and Th showed a weak deficit, but the depletion of C7, C4, and A14-2 were relatively strong. The transitional elements are the trace elements with affinity to mafic rock. Among the transitional elements (V, Cr, Ni, and Sc) in this study, element V has weak depletion to weak enrichment, while the contents of Cr, Ni, and Sc were relatively low compared to UCC. The overall demonstration showed the characteristics of relative depletion.

The value of the total amount of rare earth elements (ΣREE) ranged from 245.2×10^{-6} to 363.0×10^{-6}, with the average level of 280.4×10^{-6}, which was higher than the Laiyang Group of the lower strata (153.00×10^{-6} to 254.38×10^{-6}). Most samples' light rare earth element (LREE) content was higher, and the heavy rare earth element (HREE) content of the majority of samples was higher than UCC, but it showed a state of weak enrichment to depletion compared with PAAS. However, A14–2 showed substantial depletion with UCC and PASS. The mean value of LREE/HREE was 11.1, which was higher than that of the lower strata of the Laiyang Group (10.21) (Zhang et al., 2017) and also higher than the ratio of PAAS (9.49) and UCC (9.56). It revealed that the REE in the study area is firmly enriched, especially the LREE (**Figure 5B**). The average value of (La/Sm)N was 0.93, more diminutive than PAAS, while (Gd/Yb)N was 1.57, higher than PAAS, indicating that the samples had lower LREE and higher HREE with differential degrees than PAAS. Moreover, the closer the sample is to the sandstone block, the higher the $(La/Sm)_N$ value and the lower the $(Gd/Yb)_N$ value are. At A14-2, the value of $(La/Sm)_N$ was as high as 1.18, and the value of $(Gd/Yb)_N$ was as low as 1.43, indicating that both heavy and light rare earth elements had a high degree of differentiation.

All the samples showed a positive Eu anomaly (δEu = 1.10–1.66, mean = 1.28), which was more distinct than the lower part of the Laiyang Group, Lingshan Island (mean = 1.11) (Zhang et al., 2017), and negative Ce anomaly (δCe = 0.86–0.92, mean = 0.89).

But in this test, all the sandstone and igneous rock samples showed intense abnormal loss of Ba element, the content of which was only one-tenth of the previously measured values in the study area. Hence, it was considered a high outlier and was not involved in this study.

4.3 Geochemical Characteristics of Igneous Rock Samples

The composition of breccia (**Figure 2**) in the Laohuzui section is a metamorphic rock and igneous rock, and the metamorphic gravel is mainly gneiss. However, gneiss gravel is developed throughout the entire Laiyang Group (Li et al., 2008), so it is unlikely to use metamorphic rocks for the provenance analysis. In the research area, the Early Cretaceous volcanic activity is mainly developed in the Qingshan Group, while the volcanic activity during the sedimentary period of the Laiyang Group is relatively weak. Only volcanic rocks and volcanic breccia are developed on the top of the Haiyang area (Ren et al., 2008) and in the Shichang-Zhonglou sag (Zhou, 1999). Therefore, compared with the metamorphic breccia, the distribution of volcanic breccia in the Laiyang Group is more specific, accurately reflecting the research area's source.

The element content of igneous gravel in the study area contained higher total alkali (K_2O+ Na_2O = 6.74–7.78%) and lower SiO_2 content (43.47–56.82%, with an average of 49.68%), indicating that it is characterized by alkaline basalt. The CaO content of 4.70–8.95%, high Al_2O_3 content (15.98–20.01%, mean value 18.1%), and low Mg* value (0.38–0.44) and Ni value (23.4–59.0%) indicated that crustal mixing occurs, but not primary magma. After adjustment for loss on ignition, and cultellation at the TSA diagram (**Figure 6**) (Bas et al., 1986), it was shown that A12 was basanite, A3 was trachyandesite, and A4 and A14-1 were basaltic trachyandesite.

5 DISCUSSION

Vertically, the geochemical data of the Laohuzui section are different from the other Laiyang Group stratum on Lingshan Island (Zhang et al., 2017). Transversely, there are also significant differences in geochemical data among samples inside the Laohuzui section. Therefore, an analysis of the sample's geochemical properties is needed to understand the relationship between the sediment and the source area.

5.1 Sedimentary Cycle and Weathering Conditions in Provenance Areas

In this study, we use the value of index component variation (ICV) (Cox et al., 1995) to reflect the content of clay minerals and the amount of detrital input in the sedimentary cycle. The ICV value of the Laohuzui section was 0.83–1.15, with an average value of 1.0. Meanwhile, those of C2, C3, C4, and A14-2 were greater than 1. The ICV values for all the samples were much smaller than the rest of the Laiyang Group of the Lingshan Island section (mean value of 1.67) (Zhang et al., 2017). These data indicated that the primary cyclic sediments are still the major provenance of the Laohuzui section, but there is apparent recirculation sediment in the vicinity of the slump deposit.

The Na, K, Ca, and other alkali metal elements among feldspar minerals losses with the surface fluid, and clay minerals are formed simultaneously. During this process, the molar fraction of Al_2O_3 varies with the chemical weathering intensity (Wedepohl et al., 1969). Based on this, the Chemical Alteration Index (CIA) was proposed (Nesbitt and Young, 1982) as an indicator to reflect the degree of weathering in the provenance. The CIA values of the sandstone samples in the

Laohuzui section were 58.2–71.6, with an average value of 65.0. The sample data belonged to the region of medium chemical weathering, which was higher than other sections in the Laiyang Group, Lingshan Island (mean value of 62.6) (Zhang et al., 2017).

CIA values can be represented by either numerical values or Al_2O_3-(CaO + Na_2O)-K_2O (A-CN-K) diagrams (Nesbitt and Young, 1982). From the A-CN-K diagram, the weathering trend line of the provenance was calculated and plotted, and after obtaining the weathering trend line, the composition of the provenance was determined in turn. In **Figure 7A**, the general distribution trend of the Laohuzui section sample data was similar to that of the lower strata of the Laiyang Group. Potash feldspathization formed during diagenesis can decrease the CIA value, which is the main reason for data deviation from the ideal weathering trend (IWT) (Nesbitt and Young, 1984). Therefore, the trend line changes in Figure 7a indicate that potash feldspathization is more developed in the Laohuzui section. The evolution line formed by CIA values and sample data in the A-CN-K diagram suggests that the sediments in the Laohuzui section of Lingshan Island are still derived from unstable weathering conditions and active tectonic settings. However, the tectonic activity in the provenance is somewhat weakened compared with other sections in the Laiyang Group, Lingshan Island.

The K_2O–Rb discriminant map (Di Leo et al., 2002) was also used to distinguish the provenance compositions, and the plotted point showed that the Laohuzui section is significantly more inclined to be the provenance of pyroclastic deposits (**Figure 7B**). In sediment circulation, U significantly decreased when Th remained unchanged. Thus, Th/U can judge the weathering degree of samples (McLennan et al., 1993). The mean Th/U ratio of the Laohuzui section was 4.84 with a minimum value of 3.37 and the maximum value of 6.57, which was higher than UCC and other sections in the Laiyang Group, Lingshan Island (3.19) (Zhang et al., 2017), similar to PAAS. These data also reflect a higher weathering degree in the source area. K_2O/Al_2O_3 was between 0.18 and 0.30, and Ga/Rb was between 0.17 and 0.29, reflecting the conditions of weak weathering in the source region (Roy & Roser, 2013).

In conclusion, during the depositional period of the Laohuzui section, weathering is weak. Therefore, the main controlling factor of sediment composition is the geological environment of the provenance area. So, the geochemical data analysis of the section can be used as tracer evidence of the provenance area. The analysis results showed that the provenance of the Laohuzui section was generally consistent with the lower strata of the Laiyang Group, Lingshan Island. However, the weathering of provenance for each sample was more significant than in other sections of this region, and the degree of weathering was significantly different between each sample, which showed that closer to the slump structures, the weathering degree is stronger. Thus, the provenance of the slump structures is different from that of the lower strata of the Laiyang Group. The sediment slump structures receive input from a more weathered and more stable tectonic environment area. This phenomenon is probably related to the tectonic inversion between the Laiyang Group and the Qingshan Group.

5.2 Provenance Component Analysis

The geochemical characteristics of detrital rocks can comprehensively reflect the sediment provenance, denudation, and transportation process. Although the weathering degree of the lower strata for the Laiyang Group in Lingshan Island was increased, the provenance was still dominated by immature sediments (SiO2/Al2O3 < 6), and the weathering degree was low (CIA <70). Therefore, the geochemical properties of the Laohuzui section samples represent the provenance properties of the Laohuzui section to a large extent.

As an inactive element, Ti almost does not differentiate from Al during deposition (Hayashi et al., 1997). Therefore, Al_2O_3/TiO_2 can effectively reflect the lithology of the sedimentary provenance: the Al_2O_3/TiO_2 ranges of the mafic rocks, mafic–felsic transition igneous rocks, and felsic end-member igneous rocks were 3–8, 8–21, and 21–70, respectively (Hayashi et al., 1997). The ratio of Al_2O_3/TiO_2 in the Laohuzui section was 21.18–33.14, with an average value of 24.59, which is lower than that in the lower part of the Laiyang Group (mean value of 31.01) (Zhang et al., 2017) and still belongs to the felsic end-member provenance (21–70). The major element provenance discriminant plot (Roser and Korsch, 1988) can also discriminate provenance properties. The Laohuzui siltstone samples of Lingshan Island were mainly plotted in zone P3, while the samples C8 and C5 were in zone P4 (**Figure 8A**), indicating that the Laohuzui section mainly originates from the acidic igneous zone, with the addition of small part of the ancient sediments, similar to the rest of the Laiyang Group section.

The contents of transitional elements in the siltstone generally revealed a weak deficit, but the deficit degree is weaker than that in the lower strata of the Laiyang Group. At the same time, V presented a weak enrichment phenomenon, indicating that compared with the lower strata of the Laiyang Group, the content of mafic rock in the provenance of Laohuzui siltstone increased.

In the provenances of felsic and mafic rocks, the contents of elements such as La, Th, and Hf were significantly different, and the properties are stable. Therefore, the composition of provenance can be inferred by analyzing the contents and ratios (Cullers, 1995). In the La/Th-Hf provenance attribute discrimination diagram (**Figure 8B**), the sample points of the Laohuzui section were mainly distributed in the provenance of felsic and basic rock mixture, which is different from the lower strata of the Laiyang Group concentrated in the source area of felsic provenance. Moreover, from the bottom-up, the samples showed an increasing trend of basic rock provenance, and C4 had the highest content of basal matter source, which comes from the center of the olistolite. This change shows that the provenance changes gradually during the deposition, and the provenance changes from felsic to the mixture of felsic and basic rocks, indicating that the provenance of the olistolite is mainly basic rock.

The geochemical behavior of Eu is different from that of other trivalent REEs, which results in the positive or negative anomaly of Eu (Ding et al., 2003). Most of the feldspar developed rocks,

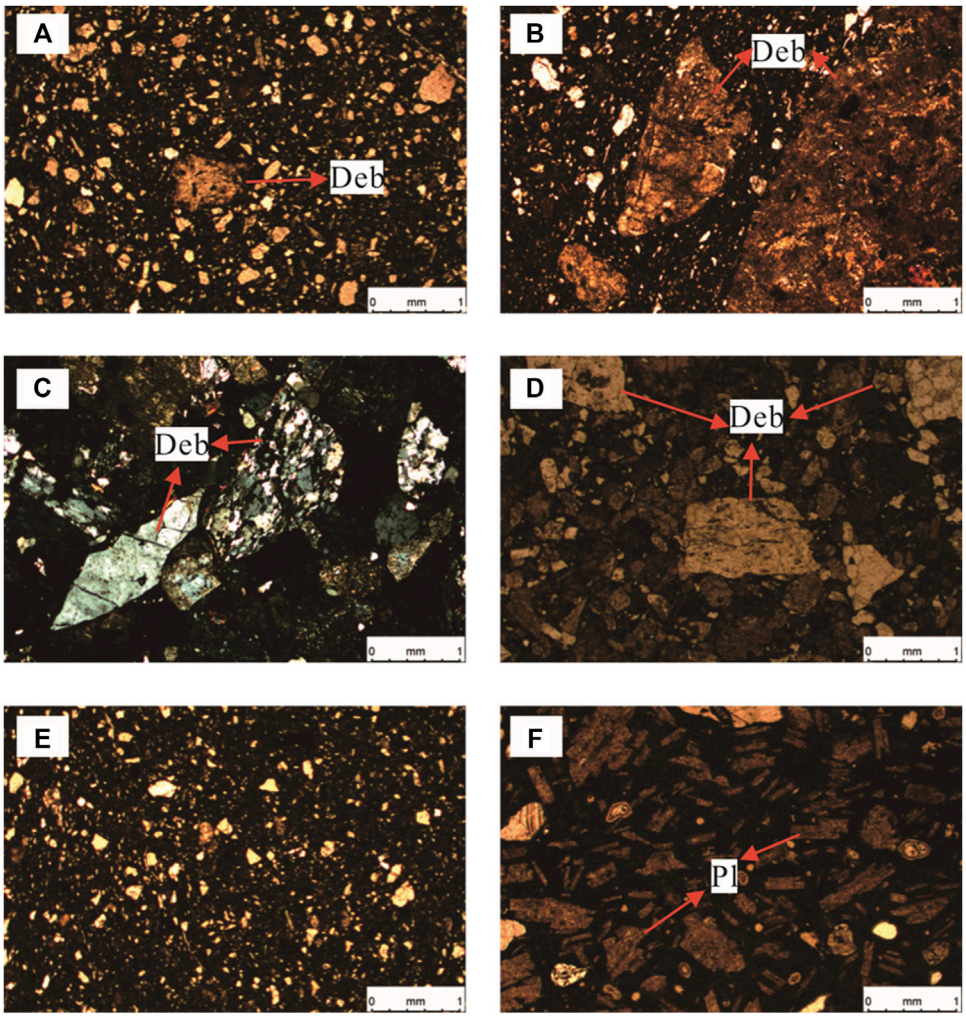

FIGURE 4 | Typical microscopic features of the Laohuzui section. **(A)** Microscopic characteristics of the lower sample of the olistolite (c1–2) (plane-polarized light). **(B)** Microscopic characteristics of hybrid sediment samples (C2) (plane-polarized light). **(C)** Microscopic characteristics of gravel samples from the olistolite (C7) (cross-polarized light). **(D)** Microscopic characteristics of sandstone block samples (C4) (plane-polarized light). **(E)** Microscopic characteristics of the upper sample of the olistolite (C5) (plane-polarized light). **(F)** Microscopic characteristics of igneous gravel samples (A12) (plane-polarized light). Deb: debris, Pl: plagioclase.

such as granites, felsic metamorphic rocks, and sedimentary rocks from continental provenance, have obvious Eu negative anomalies (Zhao et al., 2013; Tian et al., 2015). The δEu value of the Laohuzui section samples was 1.10–1.66, with an average value of 1.28, indicating a medium positive anomaly. This demonstrated that there was an addition of basal and ultrabasic source rocks in the provenance during the sedimentary section period, which were different from the felsic provenance from the lower part of the Laiyang Group (with an average value of 0.70).

Sediments can well inherit REE characteristics of rocks in the provenance. Thus, they are suitable for judging the properties of the source area. The LREE/HREE ratio (average of 11.1) for the Laohuzui section is higher than that of the lower strata (10.2) for the Laiyang Group, Lingshan Island, which indicated that compared with the lower strata, the Laohuzui section is mixed with the basic rock provenance.

The La/Sc and Co/Th ratios can effectively reflect the average components of the provenance with different chemical components (Taylor and McLennan, 1985). The La/Sc values of all samples in the Laohuzui section were distributed in 4.33–5.75, and the Co/Th values were distributed in 2.18–4.37, all of which are larger than the lower section of the Laiyang Group (La/Sc: 3.4–4.5; Co/Th: 0.69–1.99) (Zhang et al., 2017). The Co/Th–La/Sc diagram (**Figure 8C**) shows that the Laohuzui section provenance is an obvious mixture source.

5.3 Provenance of Tectonic Setting Analysis

The geochemical composition of clastic rocks can represent the properties of provenance and the tectonic setting of the formation of clastic source rocks. The use of geochemical composition to identify the tectonic setting of sedimentary basins has a long history (Mader and Neubauer, 2004; Yan et al., 2006; Song et al., 2013; Wu and Fu, 2014).

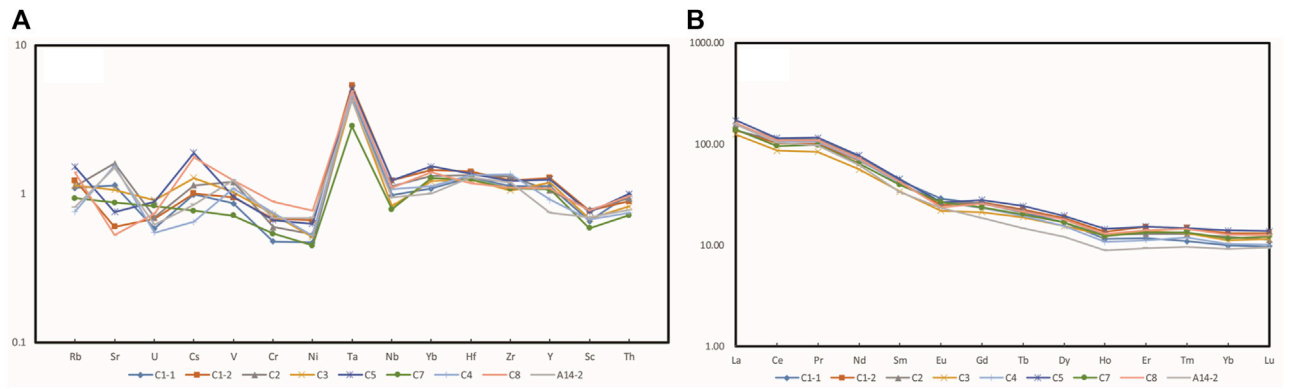

FIGURE 5 | (A) UCC microelement standardization diagram of siltstone. UCC values refer to Rudnick and Gao (2003). **(B)** Chondrite REE standardization diagram of siltstone. Chondrite values refer to Taylor and McLennan (1985).

5.3.1 Siltstone Tectonic Setting Analysis

The SiO_2/Al_2O_3–K_2O/Na_2O diagram (**Figure 9A**) (Maynard et al., 1982) shows that all the samples of the Laohuzui section were cast into A1 (island arc of basaltic and andesitic detrital), except for the points of C3 and C7, which were cast into active continental margin (ACM). It indicates that the provenance is mainly felsic provenance, with a few active continental margin sources mixed in.

The SiO_2–K_2O/Na_2O tectonic setting discrimination diagram (Roser and Korsch, 1986) shows (**Figure 9B**) that the plotted points were mainly distributed in the active continental margin, while C4 and C2 were in the oceanic island arc provenance. Compared with the lower strata of the Laiyang Group, the provenance is obviously inclined to the active continental margin.

The tectonic setting discrimination diagrams of Al_2O_3/SiO_2-(FeO + MgO)/(SiO_2+K_2O + Na_2O) (**Figure 9C**) (Kumon and Kiminami, 1994) can well reflect the sedimentary tectonic environment of the provenance. The immature island arc (IIA), evolutionary island arc (EIA), and mature magma arc (MMA) in Figure 9c are equivalent to the oceanic island arc, continental island arc, and active continental marginal environment, respectively (Bai et al., 2007). It was also observed that the provenance of sediments from the lower strata of the Laiyang Group to the Laohuzui section has gradually transformed from the island arc environment to the active continental margin environment.

La, Th, and Zr are strongly incompatible elements, while Sc and Co are strongly compatible elements. All the aforementioned elements are weak mobility elements, difficult to dissolve, and can be completely transferred to clastic rock deposits during weathering, transportation, and deposition. Therefore, they can well reflect the geochemical properties of provenance, and their content and ratio can be used to determine the nature of the source area (Taylor & McLennan, 1985; Bhatia and Crook, 1986; McLennan et al., 1990; Gu et al., 1994; Gu, 1996). A series of element discriminant diagrams have been established accordingly (Bhatia and Crook, 1986; Girty et al., 1993), reflecting that compared with the lower strata of the Laiyang Group of the Lingshan Island, the provenances of the Laohuzui section are relatively mixed. The Th–Co–Zr/10 diagram (**Figure 10A**) shows that the Laohuzui section is dominated by the oceanic island arc, while the Th–Sc–Zr/10 diagram (**Figure 10B**) is around the continental island arc, and the La–Th–Sc (**Figure 10C**) is not in the discrimination area. The La–Th–Sc diagram (**Figure 10D**) places the points in the passive continental margin.

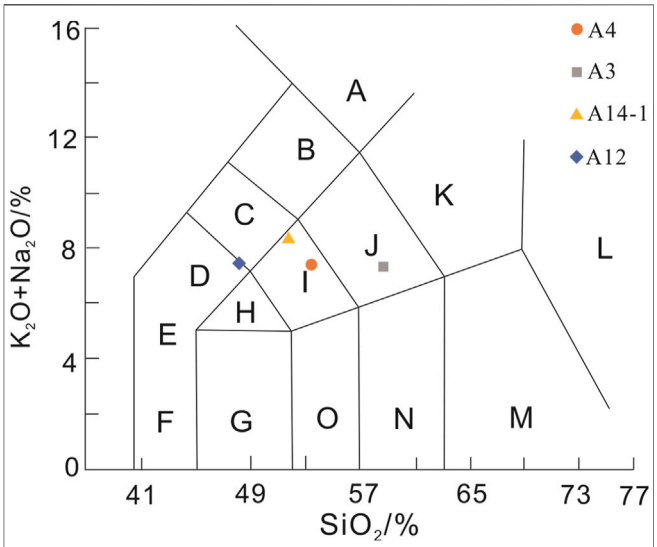

FIGURE 6 | TSA diagram of igneous rock samples, after Bas et al. (1986). (A-phonolite, B-tephriphonolite, C-phonotephrite, E-tephrite, F-picrobasalt, G-basalt, H-trachybasalt, I-basaltic trachyandesite J-trachyandesite, K-trachyte, L-rhyolite, M-dacite, N-andesite, and O-basaltic andesite.)

The trace elements and REE parameters have different distribution characteristics under different tectonic settings. Among them, the characteristic trace elements and their ratio parameters with the most discriminant significance can sensitively reveal the sediment characteristics of different tectonic settings (Bhatia, 1985; Bhatia and Crook, 1986)

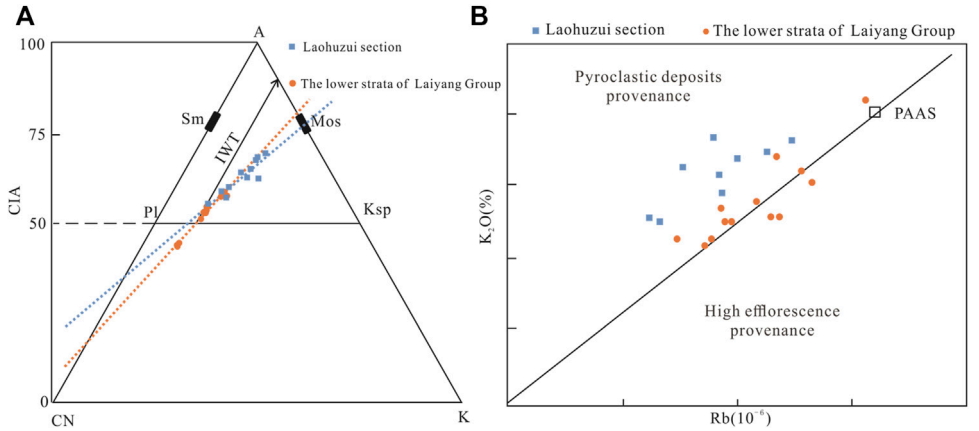

FIGURE 7 | Weathering degree discrimination diagram of the Laohuzui section and the lower strata of the Laiyang Group. **(A)** Al_2O_3-(CaO + Na_2O)-K_2O molecular proportion for siltstone, Sm: montmorillonite; Mos: illite; Pl: plagioclase; and Ksp: potassium feldspar, modified from Nesbitt and Young (1982). **(B)** K_2O–Rb discrimination diagram for the provenance of siltstones, after Di Leo et al. (2002).

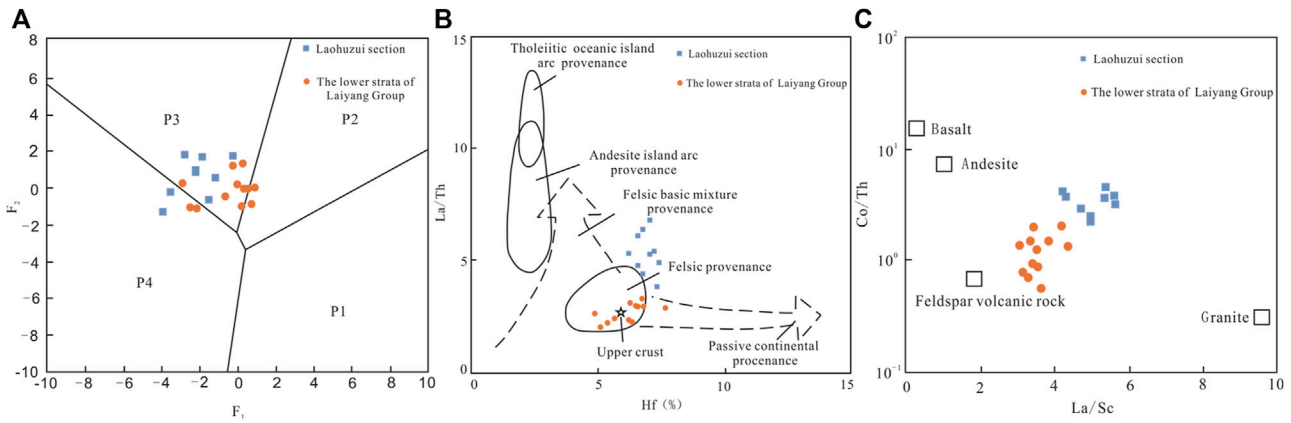

FIGURE 8 | Identification of provenance in the Laohuzui section. **(A)** Main element provenance discriminant plot, the F1 and F2 computing method and the fields of different tectonic settings are from Roser and Korsch (1988). **(B)** La/Th–Hf plot for the provenance of the siltstone, after Floyd and Leveridge (1987). **(C)** Co/Th–La/Sc plot for the provenance of the siltstone, after Gu et al. (2002).

(**Table 2**). The contents of elements in the Laohuzui section sandstone were compared with the relevant parameters in an oceanic island arc, continental island arc, active continental margin, and passive continental margin. The results showed some variation, but the provenance mainly comes from the continental island arc provenance, followed by the active continental margin provenance; few oceanic island arc provenances exist.

The aforementioned studies demonstrated differences in the conclusions of the tectonic environment discrimination of the detrital rocks in the Laohuzui section. The features of major elements showed that the island arc environment is the main provenance, partly reflecting the features of continental margin deposition, and the closer it is to the center of the slump deposit, the more obvious the features of continental margin deposition are. The trace element characteristics and the discrimination map revealed that the provenance comes from various sedimentary environments, but the continental island arc environment is the main one. In conclusion, the provenance of the Laohuzui section is relatively mixed, which is mainly island arc provenance and mixed with provenance such as active continental margin. Compared with the lower strata deposits of the Laiyang Group, where almost all provenances come from the continental island arc, the provenance input of the Laohuzui section is significantly increased.

5.3.2 Igneous Rocks Tectonic Setting Analysis

Igneous rock and metamorphic rock gravel in sedimentary rocks may record the provenance's past material composition and evolutionary history, which is an essential indicator of the source area. In the chondrite meteorites standardization (**Figure 11B**), the samples showed the LREE enrichment

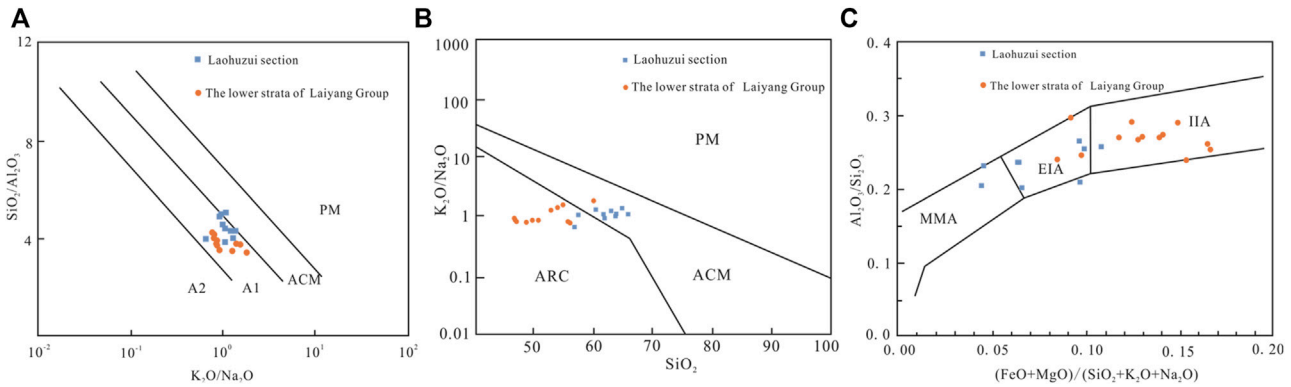

FIGURE 9 | Tectonic setting discrimination diagram of main element provenance of Laohuzui section siltstone. **(A)** K_2O/Na_2O–SiO_2/Al_2O_3 discrimination diagram for provenance tectonic setting of siltstones in the Lingshan Island, after Maynard et al. (1982); **(B)** SiO_2–K_2O/Na_2O discrimination diagram for provenance tectonic setting of siltstones in Lingshan Island, after Roser and Korsch (1986); **(C)** tectonic setting discrimination diagrams of Al_2O_3/SiO_2-(FeO + MgO)/(SiO_2 +K_2O + Na_2O), after Kumon and Kiminami (1994) (ARC: oceanic island arc; ACM: active continental margin; PM: passive continental margin; A1: island arc of basaltic and andesitic detrital; A2: evolved island arc of intrusive felsic rock detrital; IIA: immature island arc; EIA: evolved island arc; and MMA: mature magmatic arc).

and HREE depletion, among which LREE = 231.4–351.8, HREE = 20.9–39.9, and LREE/HREE = 7.44–11.96 $(La/Yb)_N$ = 0.93–1.91; and the samples showed Eu positive anomaly (δEu = 1.29–2.27), indicating the crystallization development in magmatic rocks and the enrichment of plagioclase. The overall distribution of rare earth elements reveals deep source magma, consistent with that seen in thin sections. In the original crustal standardization (**Figure 11A**), the high field strength element (HFSE) and large-ion lithophile element (LILE) were deficient. The mean value of (K_2O + Na_2O) was 7.17, and the Ritman index was greater than 3.5, indicating a slightly alkaline rock assemblage with typical deep fault zone volcanic rock characteristics.

The statistical analysis was performed on the igneous geochemical data of surrounding areas, and these data were compared with those in the study area. It was found that these geochemical properties of igneous rock samples were consistent with the lamprophyre wall in the lower part of the Laiyang Group, Lingshan Island, and the feldspathic alkaline rocks and diorites developed around 123 Ma in the Zhucheng-Taolin area (SiO_2 = 51.28–66.83%, K_2O + Na_2O = 5.35–9.68%, $^TFe_2O_3$ = 4.15–7.09%, and TiO_2 = 0.76–0.88%, No Eu negative anomaly); and they all have shown low Rb/Sr(<0.15), high Zr/Hf, and have the same distribution in the standardization of chondritic meteorites (Wang et al., 2015; Zhang, 2017) (**Figures 11C–F**). The aforementioned characteristics indicate that the main sources of volcanic rocks and gravel in the Laohuzui section are the same as the intrusive dike in the Lingshan Island area and igneous rocks in the Zhucheng-Taolin area. They all come from heterogeneous mantle sources and have experienced significant fractional crystallization. Spatially, the Lingshan Island area and the Zhucheng-Taolin area are located on both sides of the Jiaonan uplift, and they have similar sedimentary processes (Ni et al., 2016), suggesting that the igneous breccia in the Laohuzui section of the Early Cretaceous may have been affected by the same provenance as the western area of the Jiaonan uplift.

5.4 Sedimentary Environmental Analysis

The geochemical characteristics can reflect the sedimentary paleoenvironment through element migration during sedimentary diagenesis and explore the changes in the sediment provenance of the Laohuzui section.

5.4.1 Redox State Analysis

The water body under an anoxic environment shows Ce enrichment during the deposition process, which can be used to judge the redox state of the ancient water body. $Ce_{anom} < -0.1$ indicates the oxidation environment; otherwise, it reflects the anoxic environment (Raiswell et al., 1988; Wang X. X et al., 2014). The Ce_{anom} value of the Laohuzui section was −0.063 to 0.021 with the mean value of −0.048, greater than −0.1, indicating an anoxic environment.

Compared with Ni, in an anoxic environment, V can precipitate more effectively in organic complexes, resulting in more efficient precipitation in the form of organic complexes. The value of V/(V + Ni) > 0.46 indicates that sediments are deposited in an anoxic environment (Hatch and Leventhal, 1992). The V/(V + Ni) value of the Laohuzui section was 0.74–0.96, with the average value of 0.80, which was greater than 0.46, indicating that the sedimentary water is in a reductive environment.

5.4.2 Paleosalinity State Analysis

The higher the water salinity, the higher is the content of B ions in the sediments. Both are linearly correlated. The B contents in the freshwater, sea–land transition zone, and seawater are less than 80×10^{-6}, between 80×10^{-6} and 100×10^{-6}, and more than 100×10^{-6}, respectively (Degens et al., 1957). The B contents in the Laohuzui section ranged from 40×10^{-6} to 113×10^{-6}, with significant differences between samples. C4 and A14-2 inside the olistolite were freshwater deposits, and C1-1 and C3 from the lower part of the olistolite were saltwater deposits, while the rest of the samples were brackish water deposits; and all the salinity was

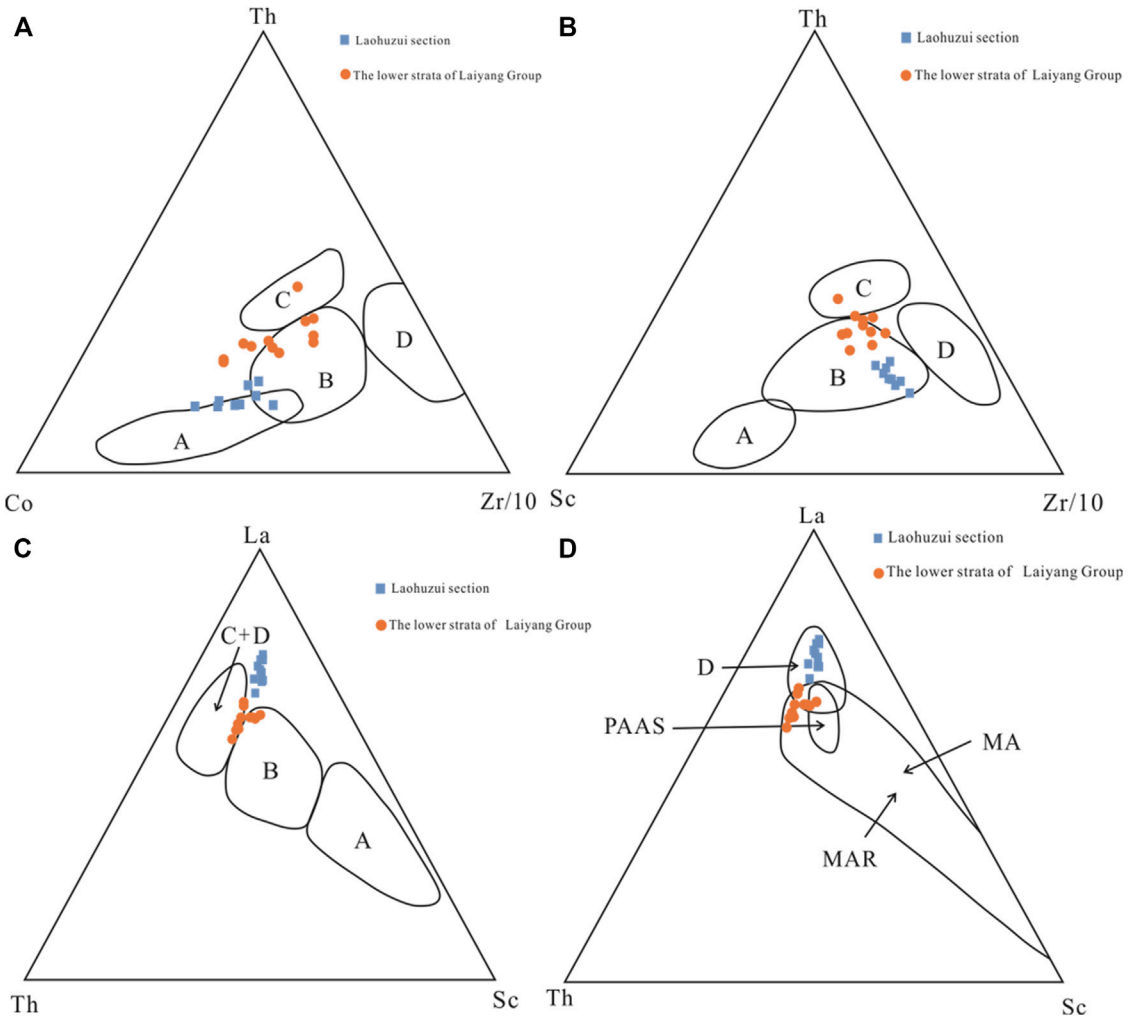

FIGURE 10 | Trace element plots of siltstones from the Laohuzui section for tectonic discrimination. **(A)** Th–Co–Zr/10 diagram, after Bhatia and Crook (1986). **(B)** Th–Sc–Zr/10 diagram, after Bhatia and Crook (1986) **(C)** La–Th–Sc, after Bhatia and Crook (1986). **(D)** La–Th–Sc diagram, after Girty et al. (1993) (PAAS: post-Archean Australian shale; MA: model andesite; MAR: magmatic arc related; **(A)** oceanic island arc; **(B)** continental island arc; **(C)** active continental margin; and **(D)** passive continental margin).

lower than that in the lower part of the Laiyang Group of Lingshan Island (average content of 149×10^{-6}). In summary, the Laohuzui section is invaded by freshwater sediment from the source of an olistolite under the sedimentary environment of saltwater.

Contrary to B, Ga is enriched in freshwater. Thus B/Ga = 4.5 is taken as the dividing line between a high-salinity saltwater environment and a freshwater environment (Wu, 2001; Li et al., 2009). The B/Ga values of the Laohuzui section were 2.25–6.56, among which those for samples C4, C2, C5, C8, and A14-2 were less than 4.5. The overall salinity of the Laohuzui section is less than that of the lower strata of the Laiyang Group, Lingshan Island (average content 6.93) (Zhang et al., 2017), which also shows the intrusion of a freshwater source of the olistolite, and the closer it is to the olistolite, the lower the salinity is.

5.4.3 Paleoclimate State Analysis

The paleoclimate discriminant diagram (**Figure 12**) (Suttner and Dutta, 1986) was used to judge the climatic environment when clastic rocks are deposited. In general, the Laohuzui is an arid–semi-arid environment.

The enrichment of elements in different climates is different. Thus, the climate index (C value) calculated based on this characteristic can be used to judge paleoclimate status (Guan, 1992; Cao et al., 2012; Feng et al., 2014; Wang et al.). The C value between 0 and 0.2 can represent an arid climate, a semi-arid climate between 0.2 and 0.4, a semi-humid climate between 0.4 and 0.6, and a humid climate greater than 0.8. The C value distribution of the Laohuzui section was 0.31–0.57, among which the C value of the slump sample was the smallest but was generally larger than the lower strata of the Laiyang Group (0.28–0.47).

TABLE 2 | Comparison of the chemical composition of sandstone in different tectonic settings in the Laohuzui section.

Oceanic island arc	Continental island arc	Active continental margin	Passive continental margin	Laohuzui section
8.2	27	37	39	50.4
19.4	59	78	85	94
11.2	28.3	35.8	42	43.8
6.9	15.1	24	16	66.4
2.3	11.1	18.8	16.7	9.1
2	8.5	10.7	7.9	12.3
96	229	179	298	228.6
2.1	6.3	6.8	10.1	6.9
19.5	14.8	8	6	9.9
131	89	48	31	99.6
18	12	10	5	29.9
89	74	52	26	79.4
45.7	36.3	26.3	29.5	33.2
48	21.5	9.5	19.1	25.4
4.3	2.4	1.8	2.2	5.6
0.5	1	1.3	1.3	2.2
0.1	0.7	0.9	1.2	0.3
2.1	4.6	4.8	5.6	4.8
0.6	1.8	4.6	6.3	5.1
0.2	0.9	2.6	3.1	0.9
1.1	0.6	0.5	0.5	0.6
56.8	19.7	15.3	6.7	25.8
0.6	0.3	0.3	0.2	0.2
4,055	1,296	1,252	681	3,484.1

Note: data of oceanic island arc, continental island arc, active continental margin, and passive continental margin are obtained from Bhatia and Crook (1986).

When the Sr/Cu value is between 1.3 and 5, the reaction area has a warm and humid climate, while when the ratio is greater than five, the climate is mainly arid and hot (Lewan and Maynard, 1982). The distribution of Sr/Cu values in the Laohuzui section was significantly different (4.64–29.22), and the ratios were the largest near the slump deposit, but both were smaller than the lower strata of the Laiyang Group. The aforementioned data showed that the strata in the Laiyang Group of Lingshan Island gradually changed from dry to wet from bottom to top, and the Laohuzui section was invaded by olistolite from an arid environment.

5.5 Tectonic Significance

The geochemical data of sediments in the Laohuzui section showed that the main provenance is the same as the lower strata of the Laiyang Group, Lingshan Island. But because of the invasion of olistolite, they have received a mixture of other provenance sediments with different properties. Moreover, the geochemical analysis showed that volcanic breccia in the Laohuzui section is similar to igneous rocks in the Zhucheng-Taolin area on the west side of the Jiaonan uplift. It is suggested that the source of the intrusion may be the same as the volcanic rocks and pyroclastic rocks developed in the Zhucheng-Taolin area.

The junction of the Laiyang Group and Qingshan Group in the Lingshan Island area is 125–128 Ma (Meng et al., 2018). A slight tectonic inversion occurred in the study area during this period. Simultaneously, the stratum has experienced rapid and substantial uplift and denudation at the top of the Laohuzui section, forming an unconformity (Dong, 2014; Zhou et al., 2018). However, the age of the upper and lower strata on the unconformity surface is basically continuous, showing that the unconformity at the junction of the Laiyang Group and Qingshan Group is not subjected to long-term and large-scale denudation.

The olistolite in the Laohuzui section has a mixed internal structure with developed mud-gravel, and the siltstone properties showed a gradual change from the bottom-up (**Figure 2**). Thus, it can be inferred that the sediment in the Laohuzui section cannot be transported too far away and may originate from the nearby orogenic belt. However, the geochemical properties of the slump sediments are quite different from other strata in the lower Laiyang Group of Lingshan Island, which indicates that the current turbidity sediments in the lower strata of the Laiyang Group are distant to the source of the olistolite and should be distant turbidite deposits.

The provenance of the Zhucheng-Taolin area in the Early Cretaceous was mainly from the Jiaonan uplift in the east, and the igneous rocks were formed around 123 Ma. The lower strata developed fluvial and lacustrine facies deposits with relatively weak tectonic activity, the upper strata had increased tectonic activity, the boundary fault was strong and volcanic breccia developed, and the climate changed from hot and humid to arid and semi-arid (Jiang and Xiong, 1993; Zhang, 2017). The sedimentary sequence showed that the provenance of sedimentary sandstone at the end of the Laiyang Group in the Zhucheng-Taolin area tends the tectonic environment to change from an active continental margin to a continental island arc environment, which indicates that the Laiyang Group in the Zhucheng-Taolin area accepted the mixing of marine sediments in the late period (Ni et al., 2016).

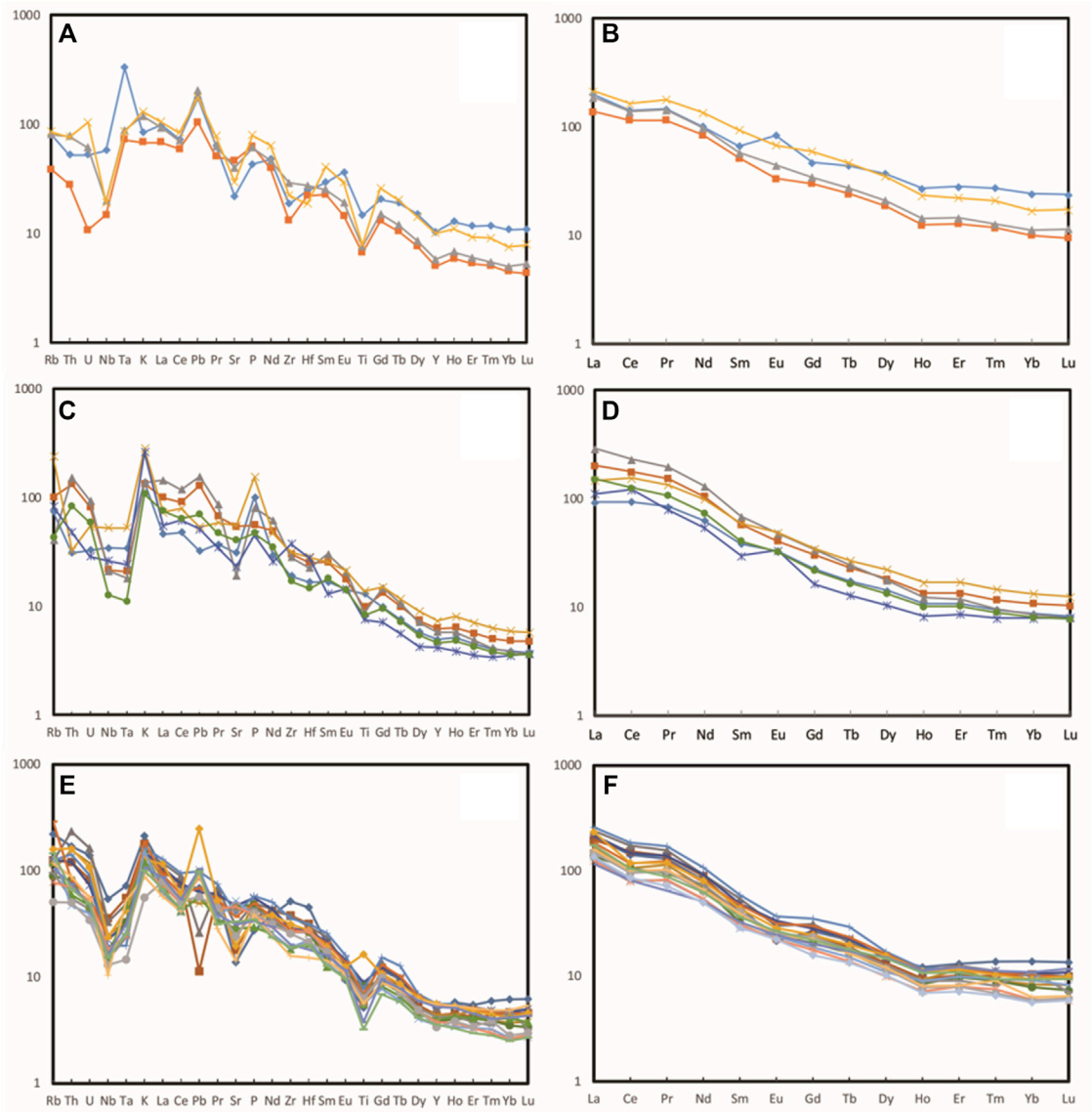

FIGURE 11 | Standardized analysis of igneous rock in the Laohuzui section and surrounding areas. **(A)** Standardization of REE chondrites in igneous rock samples from the Laohuzui section. **(B)** Original crustal standardization of trace elements in igneous rock samples from the Laohuzui section. **(C)** Standardization of REE chondrites in igneous rock samples from the lamprophyre in the lower part of the Laiyang Group, data from Wang et al. (2015). **(D)** Original crustal standardization of trace elements in igneous rock samples from the lamprophyre in the lower part of the Laiyang Group, data from Wang et al. (2015). **(E)** Standardization of REE chondrites in igneous rock samples from the Zhucheng-Taolin area, data from Zhang et al. (2017). **(F)** Original crustal standardization of trace elements in igneous rock samples from the Zhucheng-Taolin area, data from Zhang et al. (2017).

The formation and structural process of the Zhucheng-Taolin area has similar characteristics, formation time, and sedimentary form as the Laiyang Group of Lingshan Island. This feature also indicates that they share the same provenance when the Laohuzui section is deposited, in which both came from the northwestern Jiaonan uplift. In addition, it is visible from the geological map (**Figure 1**) that the Lingshan Island area and the Zhucheng-Taolin area are located on both sides of the Jiaonan uplift. This suggests that in the Early Cretaceous, both received provenance from the Jiaonan uplift and experienced the same sedimentary process. It is also consistent with previous studies that the Lingshan Island region in the Laiyang period has a relatively unified evolutionary mechanism with the Jiaolai basin (Zhou et al., 2015). Nowadays, the distance between the two is as high as 70 km, indicating that strong dislocation occurred between the Lingshan Island area and the Zhucheng-Taolin area after the olistolite deposition, which agrees with the strong sinistral strike-slip motion developed in the later period of the Laiyang Group (Zhang, 2017).

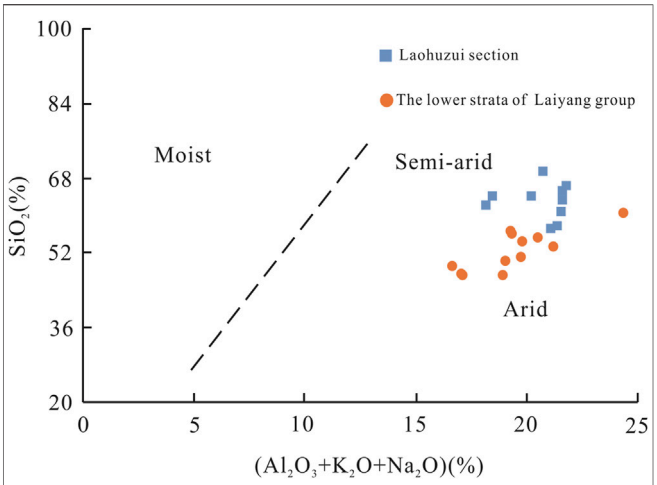

FIGURE 12 | Paleoclimate discriminant diagram, after Suttner and Dutta (1986). It shows that the Laohuzui section is an arid–semi-arid environment.

In conclusion, the sedimentary process of the Lingshan Island area at the end of the Laiyang Group has been stable in accepting distal turbidity current deposition in Early Cretaceous, forming extremely thick and stable interbedded siltstone deposit (**Figure 13A**). However, the tectonic inversion phenomenon developed at the junction of the Laiyang Group and Qingshan Group (125 Ma) is likely to lead to short and rapid stratigraphic uplift. The strong tectonic movement will lead to frequent earthquakes and the development of soft sedimentary deformation structures in the lower strata of the Laiyang Group in the Lingshan Island area. On the other hand, the slump deposit developed near the junction of the Laiyang Group and Qingshan Group (**Figure 13B**) made the strata in the Laohuzui section receive a mixture provenance from the continental margin, which is the same as the Zhucheng-Taolin area. Subsequently, through a short calm period, they continued to accept the distal turbidity current deposits (**Figure 13C**). Finally, it entered the tectonic extension period again and accepted the igneous rock deposits of the Qingshan Group (**Figure 13D**).

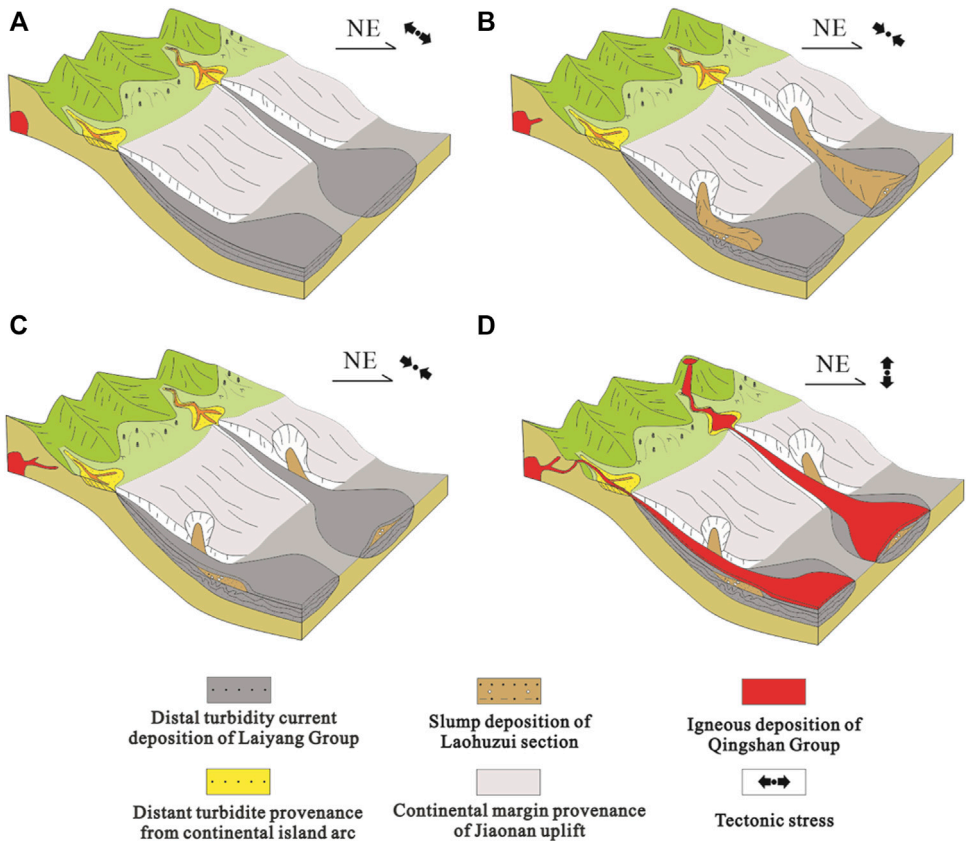

FIGURE 13 | The sedimentary model of the Laohuzui section in the Lingshan Island area. **(A)** Interbedded siltstone deposits at the end of the Laiyang Group. **(B)** Tectonic inversion developed, causing slump deposits to develop near the junction of the Laiyang Group and Qingshan Group. **(C)** During the short calm period, the Laohuzui section continued to accept the mixture provenance from a continental margin and form distal turbidity current deposits. **(D)** Tectonic extension period, when the Qingshan Group accepted the igneous rock deposits.

6 CONCLUSION

1) The large slump deposit of the Laohuzui section was developed in the tectonic inversion period between the Laiyang Group and Qingshan Group in the Lingshan Island area, showing that the closer the olistolite is, the more severe the formation deformation is. Morphologically, it showed completely different characteristics from the extremely thick turbidity current interbedded siltstone sediment developed with the soft sedimentary deformation structure in the lower part of the Laiyang Group of Lingshan Island. Compared with the sediments in the lower Laiyang Group of Lingshan Island, the sediments in the Laohuzui section showed larger particle size and higher cuttings content, igneous rock and metamorphic rock gravel development, and the closer to the olistolite, the more distinct these characteristics are.
2) A detailed study on the geochemical characteristics of the sandstone samples from the Laohuzui section showed that the provenance is similar to other strata in the Laiyang Group. The primary provenance is still the weakly weathered continental island arc provenance in the humid environment but mixed with many types of sediment from the strongly weathered continental margin in the arid environment. The changes in provenance demonstrated that the Lingshan Island area was subjected to the mixing of near-source materials from the nearby orogenic belt in the late period of the Laiyang Group, and the significant difference in the properties of the two provenances also supported that the turbidite deposit in the lower strata of the Laiyang Group in the Lingshan Island area is a distant deposit.
3) The geochemical properties of the igneous rock in the Laohuzui section olistolite are similar to the dike in the lower part of the Lingshan Island and the igneous rock deposit in the Zhucheng-Taolin area. The Lingshan Island area and the Zhucheng-Taolin area also have similar sedimentary processes. These results suggest that both were located on two sides of the same orogenic belt at the end of the Early Cretaceous, and both received provenance supplies from the Jiaonan uplift.
4) At the end of the Laiyang Group, the Lingshan Island area experienced a short and rapid tectonic uplift under the influence of tectonic inversion, transformed from the distal turbidity current sediments in the lower part of the Laiyang Group to the sediments at the junction of the Laiyang Group and the Qingshan Group, subjected the sediment at the junction to a mixture of sediment sources from the continental margin, and suffered short denudation. Subsequently, it entered the tectonic extension period again to accept the sediment of the Qingshan Group.

DATA AVAILABILITY STATEMENT

The original contributions presented in the study are included in the article/Supplementary Material; further inquiries can be directed to the corresponding author.

AUTHOR CONTRIBUTIONS

During the writing process, LQ, as corresponding author provides a specific direction and outline for this paper, as well as the necessary funding support. YY gave indispensable guidance to the content of this paper as adviser. DD and BY have provided valuable suggestions in section interpretation. DK gave valuable advice on the English translation of this manuscript. ZG played an important role in field sample collection.

FUNDING

This study was financially supported by the National Science and Technology Major Project (2017ZX05009-002: 2017ZX05072-002). The observation of the thin petrographic section thanks to the China University of Petroleum (East China).

REFERENCES

Ahmad, F., Amir, M., Adnan Quasim, M., Absar, N., and Masood Ahmad, A. H. (2022). Petrography and Geochemistry of the Middle Jurassic Fort Member Sandstone, Jaisalmer Formation, Western India: Implications for Weathering, Provenance, and Tectonic Setting. *Geol. J.* 57, 1741–1758. doi:10.1002/gj.4372

Armstrong-Altrin, J. S., Lee, Y. I., Verma, S. P., and Ramasamy, S. (2004). Geochemistry of Sandstones from the Upper Miocene Kudankulam Formation, Southern India: Implications for Provenance, Weathering, and Tectonic Setting. *J. Sediment. Res.* 74 (2), 285–297. doi:10.1306/082803740285

Bahlburg, H., Vervoort, J. D., and Dufrane, S. A. (2010). Plate Tectonic Significance of Middle Cambrian and Ordovician Siliciclastic Rocks of the Bavarian Facies, Armorican Terrane Assemblage, Germany — U–Pb and Hf Isotope Evidence from Detrital Zircons. *Gondwana Res.* 17 (2-3), 223–235. doi:10.1016/j.gr.2009.11.007

Bai, D. Y., Zhou, L., Wang, X. H., Zhang, X. Y., and Ma, T. Q. (2007). Geochemistry of Nanhuan-Cambrian Sandstones in Southeastern Hunan, and its Constraints on Neoproterozoic-Early Paleozoic Tectonic Setting of South China. *Acta Geol. Sin.* 81 (6), 755–771. doi:10.3321/j.issn:0001-5717.2007.06.004

Bas, M. J. L., Maitre, R. W. L., Streckeisen, A., and Zanettin, B.IUGS Subcommission on the Systematics of Igneous Rocks (1986). A Chemical Classification of Volcanic Rocks Based on the Total Alkali-Silica Diagram. *J. petrology* 27 (3), 745–750. doi:10.1093/petrology/27.3.745

Bhatia, M. R., and Crook, K. A. W. (1986). Trace Element Characteristics of Graywackes and Tectonic Setting Discrimination of Sedimentary Basins. *Contr. Mineral. Pet.* 92 (2), 181–193. doi:10.1007/bf00375292

Bhatia, M. R. (1983). Plate Tectonics and Geochemical Composition of Sandstones. *J. Geol.* 91 (6), 611–627. doi:10.1086/628815

Bhatia, M. R. (1985). Rare Earth Element Geochemistry of Australian Paleozoic Graywackes and Mudrocks: Provenance and Tectonic Control. *Sediment. Geol.* 45 (1-2), 97–113. doi:10.1016/0037-0738(85)90025-9

Cao, J., Wu, M., Chen, Y., Hu, K., Bian, L., Wang, L., et al. (2012). Trace and Rare Earth Element Geochemistry of Jurassic Mudstones in the Northern Qaidam Basin, Northwest China. *Geochemistry* 72 (3), 245–252. doi:10.1016/j.chemer.2011.12.002

Cox, R., Lowe, D. R., and Cullers, R. L. (1995). The Influence of Sediment Recycling and Basement Composition on Evolution of Mudrock Chemistry in the Southwestern United States. *Geochimica Cosmochimica Acta* 59 (14), 2919–2940. doi:10.1016/0016-7037(95)00185-9

Cullers, R. L. (1995). The Controls on the Major-And Trace-Element Evolution of Shales, Siltstones and Sandstones of Ordovician to Tertiary Age in the Wet Mountains Region, Colorado, USA. *Chem. Geol.* 123 (1-4), 107–131. doi:10.1016/0009-2541(95)00050-v

Degens, E., Williams, E., and Keith, M. (1957). Environmental Studies of Carboniferous Sediments Part I: Geochemical Criteria for Differentiating Marine from Freshwater Shales. *AAPG Bull.* 41 (11), 2427–2455. doi:10.1306/0bda59a5-16bd-11d7-8645000102c1865d

Di Leo, P., Dinelli, E., Mongelli, G., and Schiattarella, M. (2002). Geology and Geochemistry of Jurassic Pelagic Sediments, Scisti Silicei Formation, Southern Apennines, Italy. *Sediment. Geol.* 150 (3-4), 229–246. doi:10.1016/s0037-0738(01)00181-6

Ding, Z. J., Liu, C. Q., Yao, S. Z., Zhou, Z. G., and Yang, M. G. (2003). Geochemical Restrictions on the Source of Rare Earth Elements in the Donggouba Polymetallic Deposit. *J. Changchun Univ. Sci. Technol.* 33 (4), 437–442.

Dong, X. P. (2014). *Sedimentary Environment and Tectonic Background of the Lingshan Island in Early Cretaceous China University of Petroleum*. East China: Dong Xiaopeng.

Fan, A. P., Sun, S. N., Yang, R. C., Zhang, Z., and Yuan, J. (2019). Provenance Analysis of the Cretaceous Laiyang Group on the Lingshan Island (Western Yellow Sea, China) and its Tectono-Sedimentary Implications. *Aust. J. Earth Sci.* 67 (6), 1–17. doi:10.1080/08120099.2019.1661285

Feng, X. L., Fu, X. G., Tan, F. W., and Chen, W. B. (2014). Sedimentary Environment Characteristics of Upper Carboniferous Cameng Formation in Kongkong Chaka Area of Northern Qiangtang Basin, Tibet. *Geoscience* 28 (5), 953–961. doi:10.3969/j.issn.1000-8527.2014.05.010

Floyd, P. A., and Leveridge, B. E. (1987). Tectonic Environment of the Devonian Gramscatho Basin, South Cornwall: Framework Mode and Geochemical Evidence from Turbiditic Sandstones. *J. Geol. Soc.* 144 (4), 531–542. doi:10.1144/gsjgs.144.4.0531

Girty, G. H., Hanson, A. D., Yoshinobu, A. S., Knaack, C., and Johnson, D. (1993). Provenance of Paleozoic Mudstones in a Contact Metamorphic Aureole Determined by Rare Earth Element, Th, and Sc Analyses, Sierra Nevada, California. *Geol* 21 (4), 363–366. doi:10.1130/0091-7613(1993)021<0363:popmia>2.3.co;2

Gromet, L. P., Dymek, R., Haskin, L., and Korotev, R. (1985). The "North American Shale Composite": Its Compilation, Major and Trace Element Characteristics. *Geochimica et Cosmochimica Acta* 48 (12), 2469–2482. doi:10.1016/0016-7037(84)90298-9

Gu, B., Schmitt, J., Chen, Z., Liang, L., and McCarthy, J. F. (1994). Adsorption and Desorption of Natural Organic Matter on Iron Oxide: Mechanisms and Models. *Environ. Sci. Technol.* 28 (1), 38–46. doi:10.1021/es00050a007

Gu, X. X., Liu, J. M., Zheng, M. H., Tang, J. X., and Qi, L. (2002). Provenance and Tectonic Setting of the Proterozoic Turbidites in Hunan, South China: Geochemical Evidence. *J. Sediment. Res.* 72 (3), 393–407. doi:10.1306/081601720393

Gu, X. X. (1996). The Significance of Geochemical Characteristics of Tethys Sediments in Mesozoic to Terrestrial Weathering Conditions in Northwestern Sichuan Province. *Bull. mineralogy petrology Geochem.* 15 (1), 22–27.

Guan, Y. Z. (1992). Elemental Clay Minerals and Sedimentary Environment of Horqin Sand. *J. Desert Res.* 12 (1), 9–15.

Hatch, J., and Leventhal, J. (1992). Relationship between Inferred Redox Potential of the Depositional Environment and Geochemistry of the Upper Pennsylvanian (Missourian) Stark Shale Member of the Dennis Limestone, Wabaunsee County, Kansas, USA. *Chem. Geol.* 99 (1-3), 65–82. doi:10.1016/0009-2541(92)90031-y

Hayashi, K.-I., Fujisawa, H., Holland, H. D., and Ohmoto, H. (1997). Geochemistry of ~1.9 Ga Sedimentary Rocks from Northeastern Labrador, Canada. *Geochimica Cosmochimica Acta* 61 (19), 4115–4137. doi:10.1016/s0016-7037(97)00214-7

Jiang, Z. X., and Xiong, J. H. (1993). Sedimentation and Sedimentary Evolution of the Lower Cretaceous Laiyang Formation in Jiaolai Basin. *J. China Univ. Petroleum(Edition Nat. Sci.* 017 (002), 11–19.

Khan, Z., Quasim, M. A., Amir, M., and Ahmad, A. H. M. (2020). Provenance, Tectonic Setting, and Source Area Weathering of Middle Jurassic Siliciclastic Rocks of Chari Formation, Jumara Dome, Kachchh Basin, Western India: Sedimentological, Mineralogical, and Geochemical Constraints. *Geol. J.* 55 (5), 3537–3558. doi:10.1002/gj.3612

Kumon, F., and Kiminami, K. (1994). "Modal and Chemical Compositions of the Representative Sandstones from the Japanese Islands and Their Tectonic Implications," in *Proceedings of the 29th International Geological Congress, Part A*. Utrech, Netherlands: VSP International Science Publishers.

Lewan, M. D., and Maynard, J. B. (1982). Factors Controlling Enrichment of Vanadium and Nickel in the Bitumen of Organic Sedimentary Rocks. *Geochimica Cosmochimica Acta* 46 (12), 2547–2560.

Li, F., Qu, X. Y., Li, Liu., Yang, D. M., Wang, D. H., and Zhao, G. X. (2009). Sedimentary Environment on Upper Permian Linxi Group in Inner Mongolia. *Acta Sedimentol. Sin.* 27 (2), 265–272. doi:10.14027/j.cnki.cjxb.2009.02.004

Li, S. J., Zhang, X. Y., Zhao, X. L., Sun, Z. X., Zhang, D. Y., Zhang, L., et al. (2017). Fossils of Fishes and Conchostracan Are Found in the Lower Cretaceous of the Lingshan Island, Qingdao, Shandong Province. *Geol. Rev.* 63 (1), 1–6. doi:10.16509/j.georeview.2017.01.001

Li, S. Y., Meng, Q. R., Ren, Li. Wei., Wang, D. X., and Chu, S. W. (2008). Characteristics of Material Components from the Lower Cretaceous Laiyang Formation in Jiaolai Basin, Shangdong Province, Eastern China and Constraints to the Provenance. *Acta Petrol. Sin.* 24 (10), 2395–2406.

Lu, H. B., Wang, J., and Zhang, H. C. (2011). Discovery of Late Mesozoic Slump Deposits in the Lingshan Island, Shandong Province and Preliminary Exploration of Regional Tectonic Significance. *Acta Geol. Sin.* 85 (06), 938–946.

Lu, H. B., Zhang, H. C., Wang, J., Zhang, S. J., Dong, X. P., and Zhang, X. (2012). Giant Slippage Rocks Were Found in Late Mesozoic Turbidite in the Lingshan Island, Jiaonan, Shandong Province. *Geol. Rev.* 58 (1), 80–81. doi:10.3969/j.issn.0371-5736.2012.01.007

Lu, H. B., Zhang, H. C., Wang, J., Zhang, S. J., Dong, X. P., and Zhang, X. (2013). The Lingshan Island Early Cretaceous Flysch Stone Is Not an Intracontinental Delta Sedimentary —answer Professor Zhong Jianhua. *Geol. Rev.* 59 (1), 11–14. doi:10.3969/j.issn.0371-5736.2013.01.002

Luan, G., Li, A., Wang, J., Li, G., and Xie, R. (2010). Genetic Classification of Qingdao's Main Islands and Analysis of its Geological Environment. *Periodical ocean Univ. China* 40 (008), 111–116. doi:10.3969/j.issn.1672-5174.2010.08.018

Mader, D., and Neubauer, F. (2004). Provenance of Palaeozoic Sandstones from the Carnic Alps (Austria): Petrographic and Geochemical Indicators. *Int. J. Earth Sci.* 93 (2), 262–281. doi:10.1007/s00531-004-0391-x

Maynard, J. B., Valloni, R., and Yu, H.-S. (1982). Composition of Modern Deep-Sea Sands from Arc-Related Basins. *Geol. Soc. Lond. Spec. Publ.* 10 (1), 551–561. doi:10.1144/gsl.sp.1982.010.01.36

McLennan, S. M., Hemming, S., McDaniel, D. K., and Hanson, G. N. (1993). *Geochemical Approaches to Sedimentation, Provenance, and Tectonics*. Boulder, USA: Special Papers-Geological Society of America, 21–40. doi:10.1130/spe284-p21

McLennan, S. M., Taylor, S. R., McCulloch, M. T., and Maynard, J. B. (1990). Geochemical and Nd Sr Isotopic Composition of Deep-Sea Turbidites: Crustal Evolution and Plate Tectonic Associations. *Geochimica Cosmochimica Acta* 54 (7), 2015–2050. doi:10.1016/0016-7037(90)90269-q

Mclennan, S. M., and Taylor, S. R. (1991). Sedimentary Rocks and Crustal Evolution: Tectonic Setting and Secular Trends. *J. Geol.* 99 (1), 1–21. doi:10.1086/629470

Meng, Y. K., Li, R. H., Xu, Y., and Hou, F. H. (2018). U-Pb-Hf Isotopes and Tectonic Significance of Early Cretaceous Detrital Zircons on the Lingshan Island, Qingdao of Shandong Province. *Earth Sci.* 43 (9), 3302–3323. doi:10.3799/dqkx.2018.207

Moosavirad, S. M., Janardhana, M. R., Sethumadhav, M. S., Moghadam, M. R., and Shankara, M. (2011). Geochemistry of Lower Jurassic Shales of the Shemshak Formation, Kerman Province, Central Iran: Provenance, Source Weathering and Tectonic Setting. *Geochemistry* 71 (3), 279–288. doi:10.1016/j.chemer.2010.10.001

Nesbitt, H. W., and Young, G. M. (1982). Early Proterozoic Climates and Plate Motions Inferred from Major Element Chemistry of Lutites. *Nature* 299 (5885), 715–717. doi:10.1038/299715a0

Nesbitt, H. W., and Young, G. M. (1984). Prediction of Some Weathering Trends of Plutonic and Volcanic Rocks Based on Thermodynamic and Kinetic Considerations. *Geochimica Cosmochimica Acta* 48 (7), 1523–1534. doi:10.1016/0016-7037(84)90408-3

Ni, J. L., Zhang, H., Tang, X. L., Shi, X. X., Sun, Y. J., and Han, S. (2016). Characteristics of Major Element Geochemistry from Lower Cretaceous Sandstone in Zhucheng Basin and Their Constraint on Tectonic Setting of the Provenance. *J. Earth Sci. Environ.* 38 (5), 587–600. doi:10.3969/j.issn.1672-6561.2016.05.003

Potter, P. E. (1978). Petrology and Chemistry of Modern Big River Sands. *J. Geol.* 86 (4), 423–449. doi:10.1086/649711

Raiswell, R., Buckley, F., Berner, R. A., and Anderson, T. (1988). Degree of Pyritization of Iron as a Paleoenvironmental Indicator of Bottom-Water Oxygenation. *J. Sediment. Res.* 58 (5), 812–819. doi:10.1306/212f8e72-2b24-11d7-8648000102c1865d

Ren, F. L., Liu, Z. Q., Qiu, L. G., Han, L. G., Zhang, Y. Q., and Cao, Z. X. (2008). The Prototype Character of Jiaolai Basin in Cretaceous Laiyang Period. *Acta Sedimentol. Sin.* 26 (2), 221–233. doi:10.14027/j.cnki.cjxb.2008.02.006

Roser, B., and Korsch, R. (1988). Provenance Signatures of Sandstone-Mudstone Suites Determined Using Discriminant Function Analysis of Major-Element Data. *Chem. Geol.* 67 (1-2), 119–139. doi:10.1016/0009-2541(88)90010-1

Roser, B. P., and Korsch, R. J. (1986). Determination of Tectonic Setting of Sandstone-Mudstone Suites Using SiO2 Content and K2O/Na2O Ratio. *J. Geol.* 94 (5), 635–650. doi:10.1086/629071

Roy, D. K., and Roser, B. P. (2013). Climatic Control on the Composition of Carboniferous-Permian Gondwana Sediments, Khalaspir Basin, Bangladesh. *Gondwana Res.* 23 (3), 1163–1171. doi:10.1016/j.gr.2012.07.006

Rudnick, R. L., and Gao, S. (2003). Composition of the Continental Crust. *crust* 3, 1–64. doi:10.1016/b0-08-043751-6/03016-4

Shen, J., Zhang, B., Su, D., and Liu, C. (2016). Crustal Thickness and Poisson's Ratio Analysis of the Luxi Uplift, Yishu Fault Zone and the Jiaonan Uplift. *J. Seismol. Res.* 39 (02), 246. doi:10.3969/j.issn.1000-0666.2016.02.010

Song, C. Y., Wang, J., Fu, X. G., Feng, X. L., Zeng, S. Q., and He, L. (2013). Geochemical Characteristics and Signatures of the Sandstones from Zangxiahe Formation in Qiangtang Basin. *Earth Sci. China Univ. Geosciences* 38 (3), 508–518. doi:10.3799/dqkx.2013.051

Suttner, L. J., and Dutta, P. K. (1986). Alluvial Sandstone Composition and Paleoclimate; I, Framework Mineralogy. *J. Sediment. Res.* 56 (3), 329–345. doi:10.1306/212f8909-2b24-11d7-8648000102c1865d

Taylor, S. R., and McLennan, S. M. (1985). *The Continental Crust: Its Composition and Evolution*. United States, Chicago: University of Chicago Press.

Tian, Y., Xie, G. G., Wang, L. Z., Tu, B., Zhao, X. M., and Zeng, B. F. (2015). Provenance and Tectonic Settings of Triassic Xujiahe Formation in Qiyueshan Area,Southwest Hubei: Evidences from Petrology,Geochemistry and Zircon U-Pb Ages of Clastic Rocks. *Earth Sci. China Univ. Geosciences* 40 (12), 2021–2036. doi:10.3799/dqkx.2015.180

Wang, J., Chang, S.-C., Lu, H.-B., and Zhang, H.-C. (2014). Detrital Zircon U-Pb Age Constraints on Cretaceous Sedimentary Rocks of Lingshan Island and Implications for Tectonic Evolution of Eastern Shandong, North China. *J. Asian Earth Sci.* 96, 27–45. doi:10.1016/j.jseaes.2014.09.002

Wang, J., Chang, S.-C., Wang, K.-L., Lu, H.-B., and Zhang, H.-C. (2015). Geochronology and Geochemistry of Early Cretaceous Igneous Units from the Central Sulu Orogenic Belt: Evidence for Crustal Delamination during a Shift in the Regional Tectonic Regime. *J. Asian Earth Sci.* 112, 49–59. doi:10.1016/j.jseaes.2015.09.009

Wang, X. X., Zheng, R. C., Yan, G. Q., Wang, C. Y., and Chen, H. R. (2014). The Mudstone Sedimentary Environment and Provenance Analysis Based on the Geochemical Evidence of Rare Earth Elements:Take Chang 9 Oil-Bearing Layer in Longdong Area of Ordos Basin as an Example. *Nat. Gas. Geosci.* 25 (9), 1387–1394. doi:10.11764/j.issn.1672-1926.2014.09.1387

Wedepohl, K. H., Correns, C. W., Shaw, D. M., Turekian, K. K., and Zemann, J. (1969). *Handbook of Geochemistry*. Berlin, Heidelberg: Springer-Verlag.

Wu, S. B. (2001). Sedimentary Facies and Depositional Model of Wulabo Formation, Upper Permian Series in Bogeda Piedmont Depression, Junggar Basin. *Acta Sedimentol. Sin.* 19 (3), 333–339. doi:10.3969/j.issn.1000-0550.2001.03.003

Wu, T., and Fu, Y. (2014). Cretaceous Deepwater Lacustrine Dedimentary Sequences from the Northernmost South China Block, Qingdao, China. *J. Earth Sci.* 25 (2), 241–251. doi:10.1007/s12583-014-0418-6

Xiaoping, L., Yuan, C., Sun, M., Xiao, W., Wang, Y., Cai, K., et al. (2012). Geochemistry and Nd Isotopic Composition of the Early Paleozoic Flysch Sequence in the Chinese Altai, Central Asia: Evidence for a Northward-Derived Mafic Source and Insight into Nd Model Ages in Accretionary Orogen. *Gondwana Res.* 22, 554. doi:10.1016/j.gr.2011.04.009

Yan, Z., Wang, Z., Wang, T., Yan, Q., Xiao, W., and Li, J. (2006). Provenance and Tectonic Setting of Clastic Deposits in the Devonian Xicheng Basin, Qinling Orogen, Central China. *J. Sediment. Res.* 76 (3), 557–574. doi:10.2110/jsr.2006.046

Yang, R., Van Loon, A. J., Jin, X., Jin, Z., Han, Z., Fan, A., et al. (2019). From Divergent to Convergent Plates: Resulting Facies Shifts along the Southern and Western Margins of the Sino-Korean Plate during the Ordovician. *J. Geodyn.* 129 (SEP), 149–161. doi:10.1016/j.jog.2018.02.001

Zhang, Z. K. (2017). *The Tectono-Magmatic Evolution and Lithosphere Dynamics of Ri-Qing-Wei Basin*. East China: China University of Petroleum.

Zhang, Z. K., Zhou, Y. Q., Peng, T. M., Yu, S. S., Yue, H. W., Zhou, T. F., et al. (2017). Geochemical Characteristics and Signatures of Siltstones from Laiyang Group at the Lingshan Island,Qingdao,Shandong. *Earth Sci.* 42 (3), 357–377. doi:10.3799/dqkx.2017.027

Zhang, Z., Zhou, Y., Zhou, T., Yu, S., and Gao, F. (2018). Geochemistry of Siltstones of the Early Cretaceous Laiyang Group in Taolin Area, Shandong Province, Eastern China: Implications for Provenance, Source Weathering, Palaeo✓nvironment, and Tectonic Setting. *Geol. J.* 55 (2), 133–146. doi:10.1002/gj.3400

Zhao, M., Shao, L., Liang, J. S., Qiao, P. J., and Xiang, X. H. (2013). REE Character of Sediment from the Paleo-Red River and its Implication of Provenance. *Earth Sci. (China Univ. Geosciences)* 1, 61–69. doi:10.3799/dqkx.2013.S1.007

Zhong, J. H. (2012). Is the Mesozoic Sedimentary Rock of the Lingshan Island a Deep-Water and Far-Source Turbidite or an Intracontinental Delta Deposit?—Discuss with Professor Lu Hongbo. *Geol. Rev.* 58 (6), 1180–1182. doi:10.3969/j.issn.0371-5736.2012.06.018

Zhong, J. H., Ni, L. T., Shao, Z. F., Li, Y., Liu, X., Mao, C., et al. (2016). Tempestites and Storm Deposites in the Lower Cretaceous from the Lingshan Island,Qingdao. *J. Palaeogeogr. Ed* 22, 137–156. doi:10.13745/j.esf.2015.01.012

Zhou, J. B. (1999). Determination of the Shichang-Zhonglou Pull-Apart Basin in the Middle Section of Tanlu Fault. *Chin. J. Geol. Geol. Sinica)* 34 (1), 18–28.

Zhou, Y. Q., Zhang, Z. K., Liang, W. D., Li, S., and Yue, H. W. (2015). Late Mesozoic Tectono-Magmatic Activities and Prototype Basin Restoration in Eastern Shandong Province,China. *Earth Sci. Front.* 22 (1), 137–156. doi:10.13745/j.esf.2015.01.012

Zhou, Y. Q., Zhou, T. F., Ma, C. Q., Zhang, Z. K., Dong, S. H., Gu, Y. J., et al. (2018). Transcrustal Magmatic System of Early Cretaceous (Qingshan Stage) in Eastern Shandong and the Basin Formation Related to "Thermal Upwelling-Detachment. *Earth Sci.* 43 (10), 3373–3390. doi:10.3799/dqkx.2018.998

Conflict of Interest: The authors declare that the research was conducted in the absence of any commercial or financial relationships that could be construed as a potential conflict of interest.